

Multiphoton heralding generates large-amplitude squeezed Schrödinger cat states and parity-selective Fock superpositions from squeezed vacuum via an OPA

Yusuf Turek,^{*} Ming-Yan Sun[§], and Xiao-Xi Yao[§]
School of Physics, Liaoning University, Shenyang, Liaoning 110036, China
 (Dated: May 25, 2026)

We propose a multiphoton heralding scheme using an optical parametric amplifier (OPA) that converts squeezed vacuum into two families of non-Gaussian states: large-amplitude squeezed Schrödinger cat states and low-order parity-selective Fock superpositions. By injecting m photons into the idler port and detecting n photons at the output, effective high-order photon subtraction is realized in a single OPA device. The heralded states exhibit strong Wigner negativity and high phase-space complexity. Remarkably, under photon loss, the complexity remains substantial even after negativity vanishes, indicating a loss-resilient quantum resource. These states also surpass the Heisenberg limit in phase estimation. Our protocol establishes the OPA as a versatile platform for generating non-Gaussian states, with promising applications in loss-resilient quantum metrology and fault-tolerant quantum information processing.

I. INTRODUCTION

Gaussian states such as squeezed vacua, coherent states, and thermal states are the workhorses of continuous-variable (CV) quantum information, enabling protocols such as quantum key distribution and boson sampling [1]. However, they form a classical submanifold in phase space and are insufficient for universal CV quantum computation or fault-tolerant quantum error correction without additional non-Gaussian resources [2–4]. Non-Gaussian states, particularly Schrödinger cat (SC) states [5, 6], photon-added states [7], and Fock-state superpositions [8, 9], overcome this limitation by enabling universal gate sets [10–12], bosonic code error correction [13–16], quantum computation [17], and quantum metrology [18–21] beyond the standard quantum limit. Among these, parity-selective Fock superpositions including large-amplitude squeezed cat states are essential resources for correcting photon loss and dephasing errors [22, 23] and for encoding Gottesman-Kitaev-Preskill (GKP) qubits [24].

A standard approach to generating non-Gaussian states is conditional measurement on a beam splitter [25–28]. In that protocol, k -photon subtraction can realize a certain type of SC state with amplitude at most $\alpha \sim \sqrt{k}$ with high-fidelity. For example, single-photon subtraction from a squeezed vacuum (SV), heralded by single-photon detection, produces a small-amplitude ($\alpha \leq 1$) odd cat state with fidelity exceeding 0.99 [29–32]. For fault-tolerant bosonic error correction, however, SC states with amplitude $\alpha \geq 2$ are required to ensure near-orthogonality between the two coherent components ($e^{-2\alpha^2} \ll 1$). Achieving such amplitudes via conventional photon subtraction demands detecting at least four photons, leading to a success probability scaling as R^k with

typical beam-splitter reflectivity $R \sim 0.02 - 0.05$ which leads to extremely low generation rates [33]. Generalized photon subtraction (GPS) [34, 35], postselected weak measurement technique [36–38], distillation of squeezing [39–41] and quantum optical catalysis (QOC) [42, 43] offer improvements but remain tailored to specific target states and lack flexibility.

A promising alternative is to replace the beam splitter with an optical parametric amplifier (OPA). Unlike a beam splitter, an OPA simultaneously enables photon addition and subtraction, and its gain provides a tunable knob for state engineering. In 2019, Shringarpure and Franson showed that an OPA can prepare photon-added states without actual photon addition [44]. Our group later extended this to SV inputs with single-photon injection and detection, realizing effective two-photon subtraction and a low-order even SC state [45]. However, these schemes were restricted to single-photon idler inputs and single-photon detection.

In this work, we answer the natural question: Can multiphoton input and detection in an OPA realize effective $k \geq 3$ photon subtraction? We provide an affirmative answer. By systematically varying the number of idler input photons m and detected photons n (with SV in the signal port), we show that the OPA can effectively implement $\kappa \geq 3$ photon subtraction for $k = m + n$. Crucially, not every (m, n) pair satisfying $k = m + n$ yields a well approximation to a certain type of SC state. Only specific configurations, identified by systematically optimizing the OPA gain g and the input squeezing r , produce high-fidelity target states. For example, (1, 2) and (4, 1) generate squeezed odd Schrödinger cat (SOSC) states with amplitudes $\alpha \approx \sqrt{3}$ and $\alpha \approx \sqrt{5}$, respectively, with fidelities exceeding 0.99. These amplitudes are comparable to those achieved by four- or five-photon subtraction in conventional schemes, but with dramatically higher success probabilities (e.g., $P_{\text{trial}} \approx 1.15\%$ for (1, 2) vs $R^4 \sim 10^{-4}$ for BS subtraction). While our previous study [24] focused exclusively on the (1, 1) configuration,

[§] These authors contributed equally to this work.

^{*} Corresponding author: yusufu1984@hotmail.com

the present work extends the analysis to multiphoton input and detection, revealing a general parity selection rule and identifying optimal (m, n) pairs for generating high-fidelity SC states and higher-order Fock superpositions. Beyond state engineering, we further demonstrate the advantages of these states in phase estimation and their resilience against photon loss — aspects not considered before.

In addition to Wigner negativity, we introduce a complementary metric — phase-space complexity \mathcal{C} — to capture structural richness that can persist even when negativity vanishes under photon loss. Detailed definitions and analysis are given in Sec. III. Our protocol thus transforms the OPA from a specialized source for low-order SC states into a versatile, integrated, and reconfigurable platform for a broad class of high-photon-number non-Gaussian states.

The paper is organized as follows. After introducing the general heralding protocol in Sect. II, we analyze the properties of the heralded states from a SV input, including state engineering (Secs. III and IV) and phase estimation (Sec. V). Section VI, discusses practical limitations of our protocol. Concluding remarks are provided in Sec. VII. Numerical simulations of this work are done using QuTiP [46].

II. THE NON-GAUSSIAN STATE SOURCE

Figure 1 illustrates a generic method for generating non-Gaussian states from Gaussian and non-Gaussian inputs. In our protocol, we consider general formalism of state engineering issues by taking Gaussian and non-Gaussian inputs into two input ports of an OPA. As shown in Fig. 1, m photon ($|m\rangle$) and arbitrary state $|\phi\rangle$ are plugged into the idler and signal modes of the OPA, then OPA produces two correlated output modes. The photon-number-resolving detection (PNRD) on the idler port naturally heralds a non-Gaussian state in the signal output port. Our scheme supports multiphoton heralding, so that a much broader class of non-Gaussian states can be generated with various input states.

The OPA in our setup can be described by the two-mode squeezing unitary as

$$\begin{aligned} S(\tau) &= \exp[\tau^* ab - \tau a^\dagger b^\dagger] \\ &= \frac{1}{g} e^{-Ga^\dagger b^\dagger} g^{-(a^\dagger a + b^\dagger b)} e^{Gab} \end{aligned} \quad (1)$$

where $\tau = \rho e^{i\delta}$ and $g = \cosh \rho$ denote the non-linear and gain parameters of the OPA, $G = \tanh \tau = \sqrt{g^2 - 1}/g$, and a (a^\dagger) b (b^\dagger) are the annihilation (creation) operators of signal and idler modes, respectively. The PNRD on the idler output mode can be modelled by the projection operator

$$\Pi_n = |n\rangle\langle n| \quad (2)$$

which corresponding to the detection of n photons.



Figure 1. Schematic of the non-Gaussian source using an optical parametric amplifier (OPA). Specific states $|\phi\rangle$ — such as coherent, squeezed vacuum (SV) and small-amplitude Schrödinger cat (SC) states - are injected into the signal mode of the OPA, while m -photon is input into the idler mode of the OPA. m -photon detection at the idler output port by the photon-number-resolving detection (PNRD) heralds the generation of a non-Gaussian quantum state $|\Phi\rangle$ at the signal output. The characteristics of the output state can be controlled by adjusting squeezing parameter r , input and detected photon numbers n and m , and the gain g of the amplifier, respectively.

For our protocol, the unnormalised signal output state can be written as

$$\begin{aligned} |\psi\rangle_{m,n} &= \langle n| (\mathbb{I} \otimes \Pi_n) S(\tau) (|\phi\rangle \otimes |m\rangle) \\ &= \sum_{k=0}^m H(k, m, n) (a^\dagger)^{n-m+k} g^{-a^\dagger a} a^k |\phi\rangle, \end{aligned} \quad (3)$$

where

$$H(k, m, n) = \frac{G^{n-m+2k}}{g^{m-k+1}} \frac{(-1)^{n-m+k} \sqrt{n!m!}}{k!(n-m+k)!(m-k)!} \quad (4)$$

and the success probability is given by $P_{m,n}(n, m, r, g) = {}_{n,m}\langle \psi | \psi \rangle_{m,n}$. The specific forms of $|\psi\rangle_{m,n}$ depends on initial input signal state $|\phi\rangle$. In this work, the input signal state to the OPA is primarily the SV state, which yields the non-Gaussian heralded states that are the main focus of this paper. For completeness, we also provide the definitions of the coherent state and the SC state. The coherent state serves as a useful benchmark, while the SC state will be used as a target state in our fidelity analysis.

1. Coherent state $|\alpha\rangle$

$$\begin{aligned} |\alpha\rangle &= D(\alpha)|0\rangle \\ &= e^{-\frac{|\alpha|^2}{2}} \sum_{n=0}^{\infty} \frac{\alpha^n}{\sqrt{n!}} |n\rangle \end{aligned} \quad (5)$$

where $D(\alpha) = e^{(\alpha^* a - \alpha a^\dagger)}$ is the displacement operator and for simplicity we take α to be real.

2. SV state $|\xi\rangle$

$$|\xi\rangle = S(z)|0\rangle \quad (6)$$

where $S(z) = \exp[\frac{1}{2}(z^* a^2 - z a^{\dagger 2})]$ is the single-mode squeezing operator with a complex squeezing parameter $z = r e^{i\theta}$. In the Fock basis,

$$|\xi\rangle = \frac{1}{\sqrt{\cosh r}} \sum_{n=0}^{\infty} \frac{\sqrt{(2n)!}}{n! 2^n} (-\xi)^n |2n\rangle, \quad (7)$$

where $\xi = e^{i\theta} \tanh r$ and $\cosh r = (1 - |\xi|^2)^{1/4}$. The squeezing level in decibels (dB) is given by $-20 \log_{10}(e^{-r})$.

3. SC state $|Cat\rangle_{\theta, \alpha}$

$$|Cat\rangle_{\theta, \alpha} = N_{\theta}^{-1/2} (|\alpha\rangle + e^{i\theta} |-\alpha\rangle), \quad (8)$$

where the normalization constant is $N_{\theta} = 2(1 + e^{-2\alpha^2} \cos \theta)$. The cases $\theta = 0$ and $\theta = \pi$ correspond to even and odd SC states, respectively. The SC state is a fundamental state in CV quantum information processing, as it can be seen as a rough approximation to the GKP qubit [47].

In the recent work [48] Erlick et al. investigated the non-Gaussian state generation proposal with the same setup with ours but only considered vacuum idler input, i.e., $m = 0$. For that proposal the general form of the output state is given as (unnormalized)

$$|\psi\rangle_{0,n} = \frac{(-G)^n}{g} \frac{1}{\sqrt{n!}} (a^{\dagger})^n g^{-a^{\dagger}a} |\phi\rangle. \quad (9)$$

Since $g^{-a^{\dagger}a}$ can only modify the amplitude of a given state $|\phi\rangle \in \{|\alpha\rangle, |\xi\rangle, |Cat\rangle_{\theta, \alpha}\}$, the n -photon detection event in idler output heralds n -photon addition to the corresponding input state but with attenuated amplitudes, i.e., $|\psi\rangle_{0,n} \propto \{(a^{\dagger})^n |\frac{\alpha}{g}\rangle, (a^{\dagger})^n |\frac{\xi}{g^2}\rangle, (a^{\dagger})^n |Cat\rangle_{\theta, \alpha/g}\}$ [48]. In this process the OPA takes the role of photon addition to the given state. The special case of the above scheme is that if one consider the photon vacuum state $|0\rangle$ zero photon detection Π_0 in idler's mode (i.e., $m = n = 0$), then the OPA just takes the role of noiseless attenuation to the given input signal state [49].

In previous works, only $n = m = 1$ case has been studied for coherent state [44], SV and SC states [45], and confirmed the usefulness of OPA in non-Gaussian state generation. As an extension of previous studies, in current work, we mainly delve the multiphoton detection ($n \geq 2$) events for single photon $|1\rangle$ ($m = 1$) and $|m\rangle$ ($m \geq 2$) idler input cases.

III. GENERAL DESCRIPTION OF SV INPUT

In the following, we concentrate on the SV input. Substituting $|\phi\rangle = |\xi\rangle$ into Eq. 3 and using the properties of the squeezing operator, we obtain the unnormalized heralded state

$$\begin{aligned} |\Psi\rangle_{sv,m,n} &= \sum_{k=0}^m H(k, m, n) (a^{\dagger})^{n-m+k} g^{-a^{\dagger}a} a^k |\xi\rangle \\ &= \alpha(\xi, g) \sum_{k=0}^m H(k, m, n) g^k (a^{\dagger})^{n-m} (a^{\dagger}a)^k |\frac{\xi}{g^2}\rangle, \end{aligned} \quad (10)$$

where the factor $\alpha(\xi, g)$ is given by

$$\alpha(\xi, g) = \frac{(1 - |\xi|^2)^{1/4}}{(1 - |\frac{\xi}{g^2}|^2)^{1/4}}. \quad (11)$$

The input SV has even parity. The idler input contains m photons (parity $(-1)^m$), and the idler output is projected onto n photons (parity $(-1)^n$). Because the OPA preserves total parity, the parity of the heralded signal state must be $(-1)^{m+n}$. Consequently, the output state $|\Psi\rangle_{sv,m,n}$ contains only even Fock components when $m+n$ is even, and only odd Fock components when $m+n$ is odd. This rule is general and holds for any (m, n) .

After applying the transformation that relates the squeezed state $|\xi\rangle$, the state for $m = 1$ and arbitrary n cases can be expressed as a sum of two dominant terms:

$$\begin{aligned} |\Psi\rangle_{sv,1,n} &= \\ &(-G)^{n-1} \frac{\alpha(\xi, g)}{g^2} \sqrt{\frac{n}{(n-1)!}} \sqrt{M_{n-1}(|\frac{\xi}{g^2}|)} |\frac{\xi}{g^2}, n-1\rangle \\ &+ (-G)^{n+1} \xi \frac{\alpha(\xi, g)}{g^2 \sqrt{n!}} \sqrt{M_{n+1}(|\frac{\xi}{g^2}|)} |\frac{\xi}{g^2}, n+1\rangle, \end{aligned} \quad (12)$$

where we have defined n -photon added squeezed state

$$\begin{aligned} |\xi, n\rangle &= \frac{(a^{\dagger})^n}{\sqrt{M_n(|\xi|)}} |\xi\rangle \\ &= \frac{(1 - |\xi|^2)^{1/4}}{\sqrt{M_n(|\xi|)}} \sum_{k=0}^{\infty} (-1)^k \left(\frac{\xi}{2}\right)^k \frac{\sqrt{(2k+n)!}}{k!} |2k+n\rangle. \end{aligned} \quad (13)$$

Here the normalization factor $M_n(|\xi|)$ is expressed as:

$$M_n(|\frac{\xi}{g^2}|) = n! (1 - |\xi|^2)^{-n/2} P_n \left((1 - |\xi|^2)^{-1/2} \right), \quad (14)$$

where $P_n(x) = \frac{1}{2^n n!} \frac{d^n}{dx^n} ((x^2 - 1)^n)$ is the Legendre Polynomials.

Due to the input SV contains only even Fock components, and the operator $(a^{\dagger})^{n-1+k} g^{-a^{\dagger}a} a^k$ changes the parity by $n-1+2k$ (mode 2), the final state $|\Psi\rangle_{sv,1,n}$ contains only Fock states with parity opposite to that of n (i.e., even n yields odd Fock states, and odd n yields even Fock states). More explicitly, for odd n , the state can be written as

$$|\Psi\rangle_{sv,1,n \in \text{odd}} \propto \sum_{k=0}^{\frac{n-1}{2}} c'_{2k} |2k\rangle + \sum_{k=0}^{\frac{n+1}{2}} c''_{2k} |2k\rangle, \quad (15)$$

and for even n , the state contains only odd Fock components:

$$|\Psi\rangle_{sv,1,n \in \text{even}} \propto \sum_{k=0}^{\frac{n-1}{2}} c'_{2k+1} |2k+1\rangle + \sum_{k=0}^{\frac{n}{2}} c''_{2k} |2k+1\rangle, \quad (16)$$

The coefficients c'_k and c''_k depend on r, g and n , and can be obtained from the Eq. (12). Their explicit forms for $n = 2, 3, 4$ are given in following subsections.

As we can see, the signal output state $|\Psi\rangle_{sv,1,n}$ is a superposition of $(n-1)$ -photon and $(n+1)$ -photon added attenuated squeezed states. And if the PNRD successfully detect multi-photon ($n \geq 2$) then one can obtain the state $|\Psi\rangle_{sv,1,n}$ with success probability $P_{sv,1,n}(r, g, n) = {}_{sv,1,n}\langle\Psi|\Psi\rangle_{sv,1,n}$.

The Wigner functions of signal output state $|\Psi\rangle_{sv,m,n}$ for $m = 0, 1, 2, 3, 4, 5$ and $n = 0, 1, 2, 3, 4$ corresponding to the SV input case for fixed squeezing parameter $r = 1.0$ (≈ 8.69 dB) and OPA gain $g = 1.5$ are showed in Fig. 2. As indicated in colorful figures the non-classicality (negative region of Wigner function) of signal output states are increasing with increase the photon detection [also see the Fig. 3 (b) for this phenomena]. From these plots of phase space distribution we can speculate that similar as $n = 1$ case (studied in Ref. [45]), the multiphoton input and detection cases such as (1, 2) and (4, 1) configurations especially $n = 2$ case can also obtain very well approximated SC state, and it will confirm in following related contents.

To deeply illustrate the effects of OPA on SV state with different input and output photon configuration characterized by m and n , we investigate the complexity and negativity of our heralded states.

The Wigner negativity of a quantum state ρ is defined as [50]

$$\mathcal{N} = \int_{\mathcal{C}} |W(\alpha|\rho)| \frac{d^2\alpha}{\pi} - 1, \quad (17)$$

where $W(\alpha|\rho)$ is the Wigner function of the state ρ . This quantity characterizes the volume of the negative part of the Wigner function in phase space. It serves as a strong indicator of non-classicality: a non-zero value of \mathcal{N} signals genuine quantum interference, which is a resource for e.g. CV quantum computing. However, Wigner negativity does not very accurately capture structural features such as squeezing or high photon number when the Wigner function remains non-negative (e.g., for SV states).

In contrast, the complexity $\mathcal{C}(\rho)$ introduced by Tang et al. [51] is defined via the always-positive Husimi function $Q(\alpha|\rho) = \langle\alpha|\rho|\alpha\rangle$:

$$\mathcal{C}(\rho) = e^{S_W(\rho)-1} I(\rho) \quad (18)$$

with the Wehrl entropy

$$S_W(\rho) = - \int Q(\alpha|\rho) \ln Q(\alpha|\rho) \frac{d\alpha^2}{\pi} \quad (19)$$

and the Fisher information

$$I(\rho) = \frac{1}{4} \int \frac{||\nabla Q(\alpha|\rho)||^2}{Q(\alpha|\rho)} \frac{d\alpha^2}{\pi}. \quad (20)$$

The quantity $\mathcal{C}(\rho)$ captures the configurational trade-off between the spread (disorder) and localization (order) of the state in phase space. It is minimal ($\mathcal{C} = 1$) for all displaced thermal states (including vacuum and coherent states) and increases with squeezing and photon number. Importantly, complexity can be large even when the Wigner function is completely non-negative (e.g., SV), thus revealing a form of structural richness that is independent of negativity.

Together, Wigner negativity and complexity provide complementary insights: the former signals non-classical interference, whereas the latter quantifies the phase-space shape complexity. Their combined use allows us to distinguish, for example, a SV (high complexity, zero negativity) from a SC state (high negativity, moderate complexity) after herald-based operations.

This complementary perspective becomes particularly valuable when assessing quantum resources under realistic loss. As we will show in Sec. VI (see Fig. 14), under photon loss, \mathcal{C} decays much more slowly than Wigner negativity \mathcal{N} . Even when \mathcal{N} vanishes at sufficiently high loss rates, \mathcal{C} remains significantly above its minimal value of 1, indicating that the state retains nontrivial phase-space structure. Such structural richness can translate into practical advantages: high \mathcal{C} correlates with large QFI in phase estimation (see Sec. V), and the persistence of \mathcal{C} under loss suggests potential robustness for encoding information in fault-tolerant bosonic quantum error correction. Therefore, \mathcal{C} not only complements \mathcal{N} as a witness of non-classicality, but also serves as a more loss-resilient indicator of structural complexity relevant to quantum metrology and error correction.

Fig. 3 shows the variation of the Wigner negativity volume \mathcal{N} and complexity \mathcal{C} of the heralded quantum states generated by some different configurations of m and n with respect to the gain parameter g , under fixed initial squeezing parameter $r = 1.0$. We can see as follows: (i) As g increases, the magnitude order of both negative volume \mathcal{N} and complexity \mathcal{C} gradually increase with increasing of n ($n = 4 > n = 3 > n = 2$). This indicates that within this parameter interval, higher-order non-Gaussian operations such as $n = 3, 4$ can produce the states which possess stronger nonclassicality and more structural richness. (ii) For all n in the region where g is relatively small, the negative volume \mathcal{N} increases rapidly with the growth of g . When g increases to a certain extent, the growth of all curves slows down, eventually stabilizes, and approaches their respective saturation values, and this trend also hold for complexity \mathcal{C} .

IV. EXAMPLES WITH SPECIFIC CONFIGURATIONS

In above we have introduced the general information about multiphoton detection for SV input case. As concrete examples, in following subsections we check the concrete details of state $|\Psi\rangle_{sv,1,n}$ for $n = 2, 3, 4$ cases and

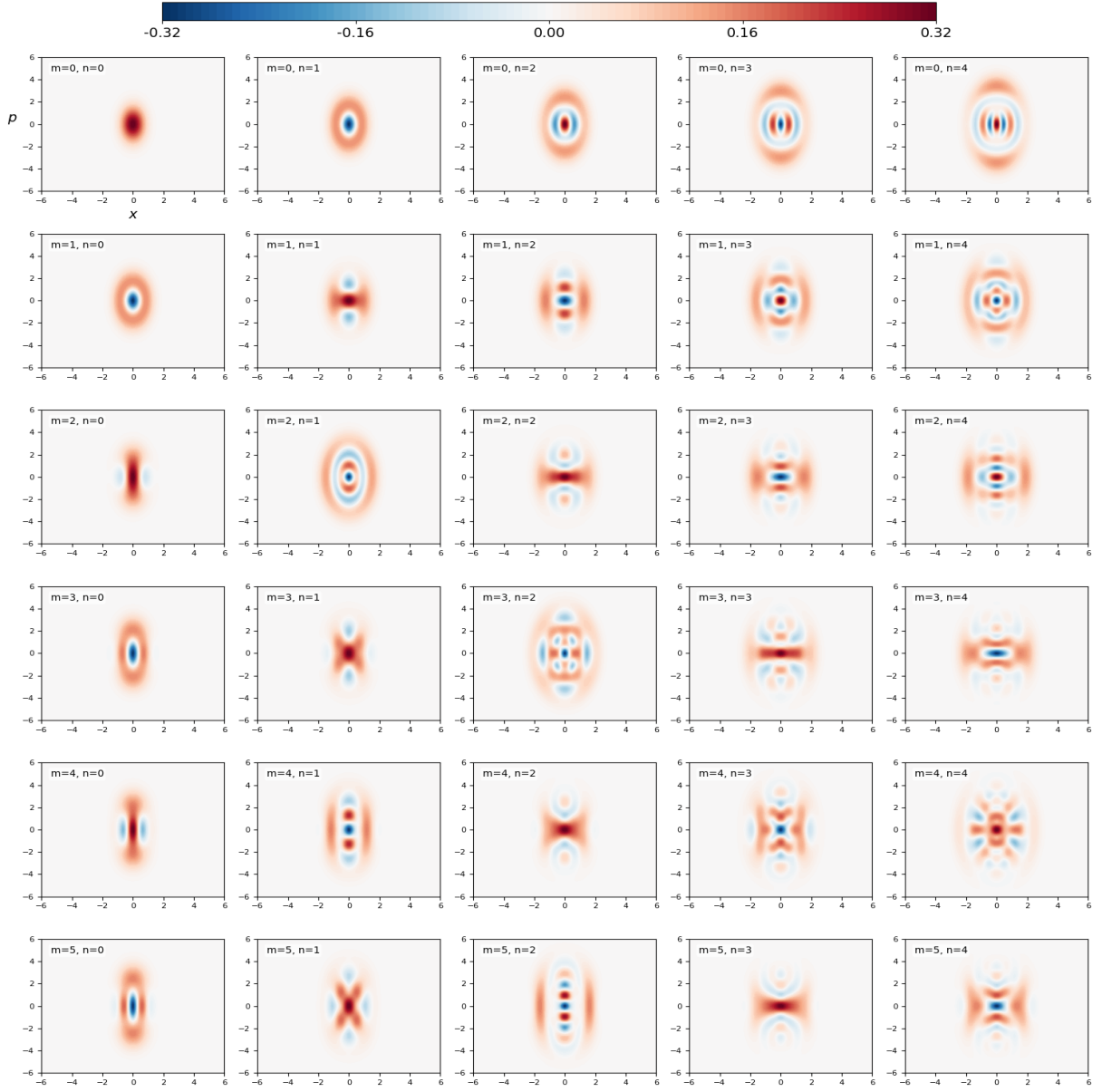


Figure 2. Wigner functions of the signal output state $|\Psi\rangle_{sv,m,n}$ for $m = 0, 1, 2, 3, 4, 5$ and $n = 0, 1, 2, 3, 4$ cases. Here we take $r = 1.0$ (≈ 8.69 dB), $\theta = \varphi = 0$ and $g = 1.5$.

investigate their related features.

A. Two-photon heralding ($n = 2$)

For two-photon detection, $\Pi_2 = |2\rangle\langle 2|$, we can obtain the corresponding signal output state as (see Eq. (12)):

$$|\Psi\rangle_{sv,1,2} = \mathcal{N}' S(\xi'') [c_1|1\rangle + c_3|3\rangle] \quad (21)$$

where $\mathcal{N}' = 1/\sqrt{|c_1|^2 + |c_3|^2}$ is the normalization constant and

$$c_1 = -\frac{\sqrt{2}}{g^2} G \lambda e^{\frac{i3}{2}\Phi(z,z')} \sqrt{\cosh r'} A + \frac{3\sqrt{2}}{2g} G^3 e^{i\theta} \sinh r \lambda e^{\frac{\phi_z(\theta')}{2} + \frac{i3}{2}\Phi(z,z')} (\cosh r')^{\frac{3}{2}} AB \quad (22a)$$

$$c_3 = -\frac{\sqrt{3}}{g} G^3 e^{i\theta} \sinh r \lambda e^{\frac{\phi_z(\theta')}{2} + \frac{i7}{2}\Phi(z,z')} (\cosh r')^{\frac{3}{2}} A^2 \quad (22b)$$

$$\zeta_1 = \tanh \frac{r}{2} e^{i\theta}; \zeta_2 = \tanh \frac{r'}{2} e^{i\varphi} \quad (22c)$$

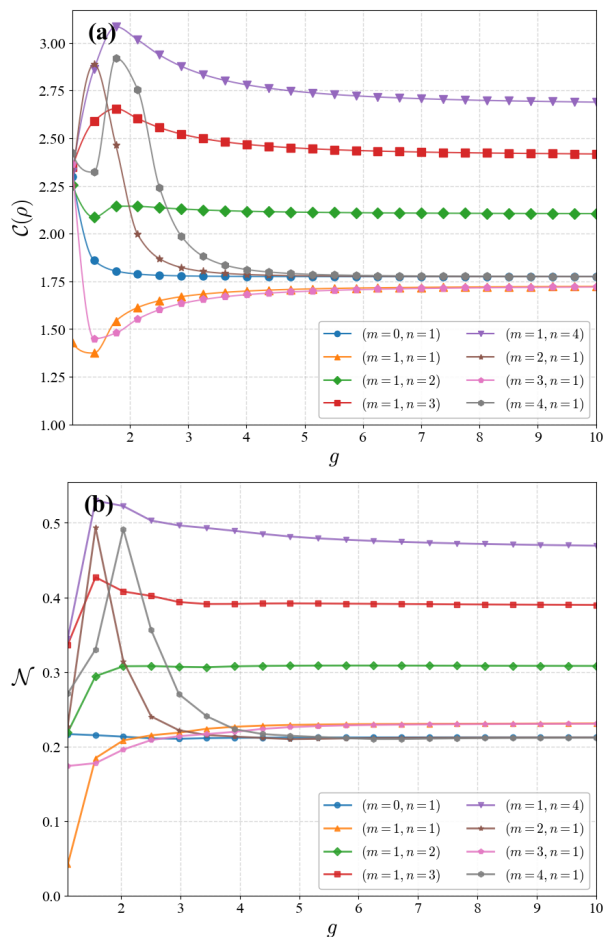


Figure 3. Complexity \mathcal{C} (a) and Wigner negativity volume \mathcal{N} (b) as a function of OPA gain g with $r = 1.0$. The other parameters are the same as in Fig. 2.

$$\Phi(z, z') = \frac{1}{i} \ln \left(\frac{1 + \zeta_1 \zeta_2^*}{1 + \zeta_1^* \zeta_2} \right), \quad z' = r' e^{i\varphi} \quad (22d)$$

$$\lambda = e^{[\ln g + \phi_z(\theta')]/2} \quad (22e)$$

$$\tanh \frac{r''}{2} e^{i\varphi''} = \frac{\zeta_1 + \zeta_2}{1 + \zeta_1 \zeta_2^*}; \xi'' = r'' e^{i\varphi''}. \quad (22f)$$

Here A and B are given as

$$\begin{aligned} A &= \cosh r \cosh r' + e^{-i(\theta-\varphi)} \sinh r \sinh r', \\ B &= \cosh r \sinh r' e^{-i\varphi} + \sinh r \cosh r' e^{-i\theta} \end{aligned} \quad (23)$$

It can be seen that the output state is the superposition of squeezed one- and three-photon number states. For $r \in (0, 1]$, the $|1\rangle$ component always larger than $|3\rangle$ component. The Wigner function of the output state $|\Psi\rangle_{sv,1,2}$ for $r = 1.0$ and $g = 1.5$ can be seen in the second

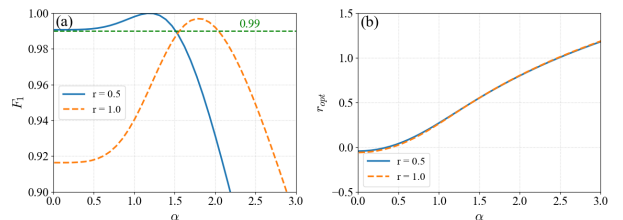


Figure 4. (a) Optimal fidelity between the output state $|\Psi\rangle_{sv,1,2}$ and the target SOSC state $|\Psi_\pi\rangle$ as a function of coherent amplitude of the target state for different squeezing parameters r . (b) Corresponding squeezing parameter γ of the target SOSC state that maximizes the fidelity in (a). The other parameters are the same as in Fig. 2.

row of the Fig. 2. As investigated in most recent work [23], our heralded state $|\Psi\rangle_{sv,1,2}$ can be used as logical codewords to correct single-photon loss and dephasing error channels in combination.

In our work we mainly discuss the similarity of our output state $|\Psi\rangle_{sv,1,n}$ to the squeezed odd or even Schrödinger cat (SOSC, SESC) states which defined as:

$$|\Psi_\theta\rangle = \mathcal{N}_\theta S(\gamma) |Cat\rangle_{\theta,\alpha}, \quad (24)$$

where the normalization coefficient is given by $\mathcal{N}_\theta = (2 + 2e^{-2\alpha^2} e^{2r} \cos \theta)^{-1/2}$, and squeezing parameter γ to be real. As previous works shown [30, 52], k -photon subtraction from the SV state, i.e., $a^k S(z)|0\rangle$, can provide a well approximation to a certain type of squeezed SC state $S(\gamma) |Cat\rangle_{k\pi,\alpha}$. In those protocols, achievable amplitude is at most $\alpha \sim \sqrt{k}$ while maintaining high fidelity. For the experimental realization of k -photon subtraction (up to 4-photons to date), please see the references listed in Table VI. Since the squeezing operation, when properly adjusted, reduces the average photon number of the SC state, the squeezed SC states can survive longer than their conventional counterparts in a lossy environment. This property makes squeezed SC states promising for a wide range of applications in quantum computing, including quantum error correction [53, 54].

In order to confirm the assumption, the fidelity between our output state $|\Psi\rangle_{sv,1,2}$ and target SOSC state $|\Psi_\pi\rangle$ can be checked as

$$\begin{aligned} F_1 &= |\langle \Psi_\pi | \Psi \rangle_{sv,1,2}|^2 \\ &= \frac{16}{9} (\nu\chi)^2 \exp\left(\frac{-2\alpha^2}{(1+g^2)}\right) \times \\ &\quad \left| \frac{g^{\frac{3}{2}} \alpha (3\sqrt{2}(1+g^2)^2 + \sqrt{3}(3-3g^4+4g^2\alpha^2)\kappa^*)}{(1+g^2)^{\frac{7}{2}}} \right|^2 \end{aligned} \quad (25)$$

with $\nu = (2-2e^{-2\alpha^2})^{-\frac{1}{2}}$, $\chi = (1+|\kappa|^2)^{-\frac{1}{2}}$ and $\kappa = c_3/c_1$.

In Fig. 4(a), the optimized fidelity F_1 corresponding the Eq. (25) as a function of coherent amplitude α of target state is plotted for different squeezing parameters

Table I. Optimized parameters of the fidelity between the output state $|\Psi'\rangle_{sv,1,2}$ and target state $|\Psi_\pi\rangle$ when the squeezing parameter of the input SV is fixed to $r = 0.74$. $\alpha = 1.732$

| g | γ | F_1 |
|------|----------|-------|
| 1.05 | 1.276 | 0.934 |
| 1.1 | 1.133 | 0.945 |
| 1.5 | 0.668 | 0.993 |
| 2.0 | 0.505 | 0.998 |
| 2.5 | 0.437 | 0.998 |
| 5 | 0.350 | 0.997 |
| 10 | 0.329 | 0.997 |

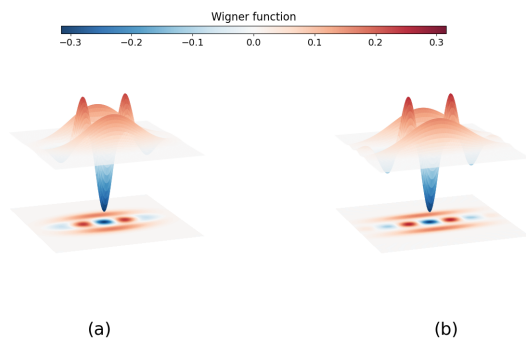


Figure 5. (a) Wigner function of the generated state with $r = 1.0$ and $g = 1.5$. (b) Wigner function of the ideal SOCS state with $\gamma = 0.803$ and $\alpha = 2.0$. Other parameters are the same as those used in Fig. 4. For these parameters, the fidelity calculated using the Wigner functions of the generated and ideal SOCS state is $F_1 = 0.992$. The other parameters are the same as in Fig. 2.

$r = 0.5$ (≈ 4.34 dB), $r = 1.0$ (≈ 8.69 dB) and the parameter g is set to 1.5. In Fig. 4 (b) the corresponding squeezing parameter γ of the target SOCS state that can give the optimized fidelity values in Fig. 4 (a) is showed. As can be observed, when $r = 0.5$ is considered, the nearly perfect fidelity $F_{max} = 0.999$ can be achieved for $\alpha = 1.191$ and $\gamma_{opt} = 0.378$. Furthermore, in $r = 1.0$ case, the maximum fidelity $F_{max} = 0.997$ is occurred to the corresponded $\alpha = 1.795$ and $\gamma_{opt} = 0.706$ [see Fig. 4(b)]. It's also interesting to note that for $r = 1.0$ case, the range of amplitude α for $F_1 > 0.99$ is from 1.565 to 2.029.

In Table I, we give the optimized parameters and corresponding fidelity F_1 for fixed squeezing parameter $r = 0.74$ and fixed amplitude $\alpha = 1.732$ while changing the gain values g from 1.01 to 10. As g increases, the optimal value of γ decreases, As we noticed, the optimal fidelity F_1 for the entire range of g remains considerable high values, $F_1 \geq 0.993$, and reached the saturating value 0.997 for $g \geq 5.0$. The numerical data in Table I indicated that our protocol with (1, 2) configuration can be equivalent to 3-photon subtraction from SV state, since $\sqrt{3} \approx 1.732$.

Figure. 5 (a) displays the Wigner function of the heralded state $|\Psi\rangle_{sv,1,2}$ for $r = 1.0$ and $g = 1.5$. The ideal

target SOCS state with $\gamma = 0.803$ and $\alpha = 2.0$ is shown in Figs. 4 (b) yielding a high fidelity $F_1 = 0.992$ to the our heralded state $|\Psi\rangle_{sv,1,2}$. The high similarity is evident from the characteristic negative Wigner region and the two positive peaks.

To explore the limits of our protocol, we further optimized the fidelity for a target SOCS state with an even larger amplitude $\alpha = 2.236$ (corresponding to $\sqrt{5}$) for regions $r \in [1, 3]$ and $g \in (1, 10]$ and found that the fidelity always in 0.983 ± 0.002 level. While this is slightly lower than the optimal fidelity achieved at $\alpha = 1.732$ (see Table I, where $F_1 \geq 0.993$), it still represents a highly competitive level of quantum state fidelity for SC states in this amplitude regime. Achieving $\alpha \geq 2$ is critical for quantum information, as it ensures near-orthogonality between the two cat-state components ($e^{-2\alpha^2} \ll 1$), enabling fault-tolerant bosonic quantum error correction [23].

Compared to traditional multiphoton subtraction, which requires detecting at least four photons to reach $\alpha \sim 2$, our scheme achieves the same with only two-photon detection and a corresponding single-trial successful probability on the order of 10^{-2} (see Sec. VI for details), significantly enhancing the success probability (scaling as R^2 vs R^4 , where $R \sim 0.02 - 0.05$ is the beam-splitter's reflectivity in conventional subtraction schemes). Moreover, our single-OPA setup is more compact than GPS schemes requiring two squeezed sources and a beam splitter. These results confirm that our two-photon heralding protocol reliably generates high-fidelity SOCS states with amplitudes $\alpha \gtrsim 2$, reaching a regime essential for fault-tolerant quantum computing while offering experimental simplicity and higher generation rates.

In addition to the ideal SOCS state, the heralded state $|\Psi\rangle_{sv,1,2}$ generated by two-photon detection exhibits excellent agreement with the target states $a^2|\Psi_\pi\rangle$. Figure. 6 (a) presents the optimized fidelity as a function of the coherent amplitude α of the target states, while Fig. 6 (b) shows the corresponding optimal squeezing parameter γ of the target state. For the parameters $g = 1.5$ and $r = 0.5$ (1.0), the optimized fidelity between $|\Psi\rangle_{sv,1,2}$ and $a^2|\Psi_\pi\rangle$ reaches $F = 0.999$ (0.982) at $\alpha = 1.399$ (1.900). For the $r = 0.5$, we observe a broad high-fidelity region ($F > 0.99$) for α ranging from 0.01 to 1.701. In contrast, when $r = 1.0$, the optimal fidelity always lower than 0.99 for entire parameter regimes. In both scenarios, the optimized coherent amplitude α increases with the gain parameter g .

B. Three-photon heralding ($n = 3$)

We now consider the case where the idler output is projected onto the Fock state $|3\rangle\langle 3|$, i.e., $\hat{\Pi} = |3\rangle_b\langle 3|$. Substituting $n = 3$ into the general expression Eq. (12) for $m = 1$ cases, we obtain the following normalized output state for the signal mode:

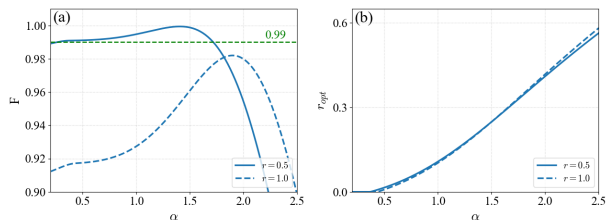


Figure 6. (a) Optimized parameters for the fidelity between $|\Psi\rangle_{sv,1,2}$ with $a^2|\Psi_\pi\rangle$ for $r = 0.5$ (solid curve) and $r = 1.0$ (dashed curve). (b) Corresponding squeezing parameter γ of the target state that maximizes the fidelity in (a). The other parameters are the same as in Fig. 2.

$$|\Psi\rangle_{sv,1,3} = \mathcal{N}'' S(\xi'') [c_0|0\rangle + c_2|2\rangle + c_4|4\rangle] \quad (26)$$

where $\mathcal{N}'' = 1/\sqrt{|c_0|^2 + |c_2|^2 + |c_4|^2}$ is the normalization constant. The complex squeezing parameter ξ'' in this final squeezing operator $S(\xi'')$ is defined in Eq. (22f), and the coefficients c_0, c_2, c_4 are given by

$$c_0 = -\frac{\sqrt{6}}{2g^2} G^2 \lambda e^{\frac{i}{2}\Phi(z,z')} \sqrt{\cosh r'} AB + \frac{\sqrt{6}}{2g} G^4 e^{i\theta} \sinh r \lambda e^{\frac{\phi_z(\theta')}{2} + \frac{i}{2}\Phi(z,z')} (\cosh r')^{\frac{3}{2}} \sinh r AB^2, \quad (27a)$$

$$c_2 = \frac{\sqrt{3}}{g^2} G^2 \lambda e^{\frac{i5}{2}\Phi(z,z')} \sqrt{\cosh r'} A^2 - \frac{2\sqrt{3}}{g} G^4 e^{i\theta} \sinh r \lambda e^{\frac{\phi_z(\theta')}{2} + \frac{i5}{2}\Phi(z,z')} (\cosh r')^{\frac{3}{2}} \sinh r A^2 B, \quad (27b)$$

$$c_4 = \frac{2}{g} G^4 e^{i\theta} \sinh r \lambda e^{\frac{\phi_z(\theta')}{2} + \frac{i9}{2}\Phi(z,z')} (\cosh r')^{\frac{3}{2}} \sinh r A^3 \quad (27c)$$

The symbols $A, B, \Phi(z, z'), \phi_z(\theta')$ and λ are defined in Eqs. (22c-22f).

From Eq. (26) we observe that the heralded state contains only even Fock components $|0\rangle, |2\rangle$ and $|4\rangle$. This is consistent with the parity argument given in above content: for odd n (here $n = 3$), the output state retains the even-parity structure of the input SV. The $|0\rangle$ component is generally very small compared to $|2\rangle$ and $|4\rangle$ for the parameter ranges considered in this work. The Wigner function of $|\Psi\rangle_{sv,1,3}$ for a representative set of parameters ($r = 1.0$ and $g = 1.5$) is shown in this second row and forth column of Fig. 2. Since the state contains only even Fock components, the Wigner function exhibits a positive central peak surrounded by negative regions at larger phase-space radii. This structure is characteristic of even-parity non-Gaussian states and differs markedly from the odd cat-like states obtained for $n = 2$.

Over the entire parameter ranges we explored ($r \in [0, 3]$ and $g \in (1, 10]$), the fidelity of the (1, 3) configuration with an ideal SESC state never exceeds 0.914, which

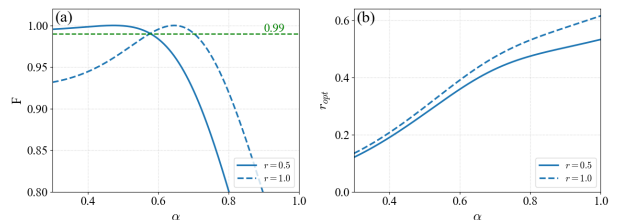


Figure 7. (a) Optimized parameters for the fidelity between $|\Psi\rangle_{sv,1,3}$ with $a^{\dagger 2}|\Psi_0\rangle$ for $r = 0.5$ (solid curve) and $r = 1.0$ (dashed curve). (b) Corresponding squeezing parameter r of the target state that maximizes the fidelity in (a). The other parameters are the same as in Fig. 2.

Table II. Optimized parameters for the fidelity between $|\Psi\rangle_{sv,1,3}$ with $|\phi_1\rangle$

| r | g | γ_{opt} | α | F |
|-----|-----|----------------|----------|-------|
| 0.5 | 1.5 | 0.250 | 0.473 | 0.999 |
| | 2.5 | 0.133 | 0.586 | |
| | 5 | 0.085 | 0.604 | |
| | 10 | 0.073 | 0.612 | |
| 1.0 | 1.5 | 0.430 | 0.645 | |
| | 2.5 | 0.233 | 0.742 | |
| | 10 | 0.120 | 0.789 | |

is substantially below the 0.970 ± 0.010 level achieved by (3,1) configuration (see Table VI). Thus (1, 3) is not a viable choice for preparing high-fidelity SESC state with amplitude $\alpha \sim 2$ (equivalent to four-photon subtraction). Instead, the (1, 3) configuration should be preferred for such tasks.

After careful consideration, we find that $|\Psi\rangle_{sv,1,3}$ exhibits high fidelity with the target state $a^{\dagger 2}|\Psi_0\rangle$. To quantify the non-Gaussian character of the three-photon heralded state $|\Psi\rangle_{sv,1,3}$ given in Eq. (26), we evaluate its overlap with the even-parity target state $a^{\dagger 2}|\Psi_0\rangle$ that naturally arise from photon operations on squeezed SC state. Figure 7 shows the optimized fidelity as a function of the target coherent amplitude α for two input squeezing parameters, $r = 0.5$ and $r = 1.0$, at fixed OPA gain $g = 1.5$. For $r = 0.5$, the fidelity can exceed 0.99 over a broad range of α and the maximum fidelity reach nearly 0.999. When r increases to 1.0 the optimal Fidelity shifts to larger α , while the peak fidelity remains above 0.99. Panel (b) displays the corresponding optimal squeezing parameter γ of the target states that maximizes the fidelity in panel (a). The γ_{opt} increases monotonically with increasing α and $r = 0.5$ case generally smaller for the larger input squeezing $r = 1.0$.

In order to further confirm the similarities of the between our heralded state $|\Psi\rangle_{sv,1,3}$ and $|\phi_1\rangle = a^{\dagger 2}|\Psi_0\rangle$, we list the optimized fidelities and parameters in Table II. For input squeezing $r = 0.5$ the fidelity reaches 0.999 for all g values from 1.5 to 10; the optimal coherent amplitude α lies between 0.473 and 0.612, while γ_{opt} decreases

from 0.250 to 0.073. For $r = 1.0$, the fidelity remains above 0.998 with $\alpha \approx 0.645 - 0.789$ and γ_{opt} ranging from 0.430 to 0.120. These results demonstrate an excellent agreement with the two-photon-added SESC state.

We also notice that the $|\phi_2\rangle = a^\dagger a |\Psi_0\rangle$ can also give well approximation to our state with (1, 3) configuration. The extreme high fidelity $F \geq 0.999$ between $|\Psi\rangle_{sv,1,3}$ and the target $|\phi_2\rangle$ is achieved for all considered OPA gain value $g \in (1, 10]$ with optimal $\alpha \in [1.063, 1.324]$ and $\gamma_{opt} \in [0.219, 0.158]$ when the input squeezing is $r = 0.5$. For $r = 1.0$, the fidelity is slightly lower (0.990 – 0.996), but the achieved coherent amplitudes are significantly larger ($\alpha \approx 1.48 - 1.69$). Thus, $|\phi_1\rangle$ provides higher fidelity, while $|\phi_2\rangle$ yields a larger SC size, offering a flexible choice depending on the experimental goal.

The high fidelity between $|\Psi\rangle_{sv,1,3}$ and the states $|\phi_1\rangle$ and $|\phi_2\rangle$ can be explained as follows. First, both target states contain only even Fock components, matching the parity of our heralded state (for odd $n = 3$, the output state retains the even parity of the input SV). Second, although the output state has a small $|0\rangle$ component, its amplitude is negligible compared to those of $|2\rangle$ and $|4\rangle$. Third, as shown in Table II, the optimal squeezing parameters γ_{opt} are small and decrease with increasing the OPA gain g (this trend is same to the $|\phi_2\rangle$ case). For such small γ , higher even Fock states ($|6\rangle, |8\rangle, \dots$) in the SCS state are substantially suppressed. Consequently, both the target states and the heralded state are dominated by the same low-lying even Fock components ($|2\rangle$ and $|4\rangle$), which explains the observed high fidelities.

C. Four-photon heralding ($n = 4$)

We now turn to the case of detecting four photons at the idler output, i.e., $\hat{\Pi} = |4\rangle\langle 4|$. Inserting $n = 4$ into the general formula Eq. (10) (with $m = 1$ fixed) yields the heralded signal state

$$|\Psi\rangle_{sv,1,4} = \mathcal{N}''' S(\xi'') [c_1|1\rangle + c_3|3\rangle + c_5|5\rangle] \quad (28)$$

where $\mathcal{N}''' = 1/\sqrt{|c_1|^2 + |c_3|^2 + |c_5|^2}$ denotes the normalization constant, and

$$c_1 = \frac{\sqrt{6}}{g^2} G^3 \lambda e^{\frac{3i}{2}\Phi(\xi, \xi')} \sqrt{\cosh r'} A^2 B + \frac{15\sqrt{6}}{12} G^5 e^{i\theta} \sinh r \lambda e^{\frac{\phi_z(\theta')}{2} + \frac{3i}{2}\Phi(\xi, \xi')} (\cosh r')^{\frac{3}{2}} A^2 B^2 \quad (29a)$$

$$c_3 = -\frac{2}{g^2} G^3 \lambda e^{\frac{7i}{2}\Phi(\xi, \xi')} \sqrt{\cosh r'} A^3 - 5A^3 B G^5 e^{i\theta} \sinh r \lambda e^{\frac{\phi_z(\theta')}{2} + \frac{7i}{2}\Phi(\xi, \xi')} (\cosh r')^{\frac{3}{2}} \quad (29b)$$

$$c_5 = \sqrt{5} G^5 e^{i\theta} \sinh r \lambda e^{\frac{\phi_z(\theta')}{2} + i\frac{11}{2}\Phi(\xi, \xi')} (\cosh r')^{\frac{3}{2}} A^4. \quad (29c)$$

A striking feature is that only odd Fock states appear — a direct consequence of parity conservation: for even n

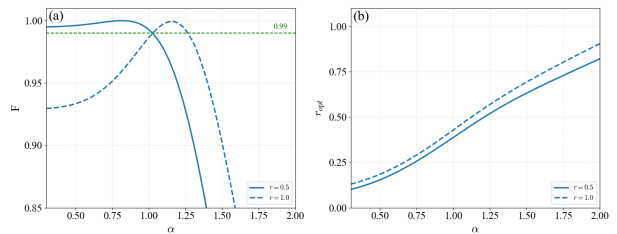


Figure 8. (a) Optimized parameters for the fidelity between $|\Psi\rangle_{sv,1,4}$ with $a^{\dagger 2}|\Psi_\pi\rangle$ for $r = 0.5$ (solid curve) and $r = 1.0$ (dashed curve). (b) Corresponding squeezing parameter r of the target state that maximizes the fidelity in (a). The other parameters are the same as in Fig. 2.

(here $n = 4$), the output state acquires odd parity relative to the input SV. The corresponding Wigner function, plotted in the fourth row fourth column of Fig. 2 for $r = 1.0$ and $g = 1.5$, shows a deep negative dip at the origin and two well-separated positive humps, reminiscent of an odd SC state but with richer structure due to the $|5\rangle$ contribution. We notice that our heralded state $|\Psi\rangle_{sv,1,4}$ also cannot be approximated to a SOSC state, as its maximum fidelity is only 0.816 over all parameter regimes we considered ($r \in [0, 3]$ and $g \in (1, 10]$).

By numerical calculation we have found that there are lots of states such as $|\psi_1\rangle = a^{\dagger 2}|\Psi_\pi\rangle$, $|\psi_2\rangle = a^{\dagger 3}a|\Psi_\pi\rangle$ and $|\psi_3\rangle = a^{\dagger 2}a^2|\Psi_\pi\rangle$ can give extreme similarities with our heralded state $|\Psi\rangle_{sv,1,4}$. Each of these contains only odd Fock components, matching the parity of our heralded state. As an concrete example, below we choose $|\psi_1\rangle$ to give the analysis about the optimal fidelity between $|\Psi\rangle_{sv,1,4}$ and $|\psi_1\rangle$.

Figure 8 (a) illustrates the optimized fidelity between the heralded state $|\Psi\rangle_{sv,1,4}$ and the target state $|\psi_1\rangle$ as a function of the target coherent amplitude α for input squeezing parameters $r = 0.5$ (solid curves) and $r = 1.0$ (dashed curves), with OPA gain fixed at $g = 1.5$. For $r = 0.5$, all the fidelity exceed 0.99 over a certain range of α . When r increases to 1.0, the optimal α shifts to larger values, and the optimal fidelity can reach above 0.99 within a very narrow region. The corresponding optimal squeezing parameter γ_{opt} of the target states versus α is shown in Fig. 8 (b). The similarity between our signal output state and $|\psi_1\rangle$ can be further confirmed by the data presented in Tables III. The data are shown for input squeezings $r = 1.0$ and $r = 1.0$ over a range of OPA gains $g = 1.5$ to 10. For $r = 0.5$, the fidelity of 0.999 or higher across the entire gain range, indicating an excellent match. The target $|\psi_1\rangle$ yields a moderate coherent amplitude α (from 0.891 to 1.049) with very high fidelity. Furthermore, for the larger input squeezing $r = 1.0$ the fidelity remains highly competitive. The fidelity stays above 0.998 with α ranging from 1.157 to 1.354.

For comparison, we also take fidelity analysis between $|\Psi\rangle_{sv,1,4}$ and other two target states $|\psi_2\rangle$ and $|\psi_3\rangle$. For $|\psi_2\rangle$, the fidelity varies between 0.983 and 0.999 with α around 0.74 – 0.79. Meanwhile, the fidelity for $|\psi_3\rangle$ is

Table III. Optimized parameters for the fidelity between the heralded state $|\Psi\rangle_{sv,1,4}$ and the target state $|\psi_1\rangle$. The input squeezing r and OPA gain g are varied; γ_{opt} and α are the optimal squeezing and coherent amplitude of the target state, respectively, and F is the corresponding fidelity.

| r | g | γ_{opt} | α | F |
|-----|-----|----------------|----------|-------|
| 0.5 | 1.5 | 0.291 | 0.891 | 0.999 |
| | 2.5 | 0.191 | 0.979 | |
| | 5 | 0.148 | 1.035 | |
| | 10 | 0.137 | 1.049 | |
| 1.0 | 1.5 | 0.518 | 1.157 | 0.998 |
| | 2.5 | 0.325 | 1.300 | |
| | 5 | 0.243 | 1.344 | |
| | 10 | 0.222 | 1.354 | |

0.998 ± 0.001 , and it produces the largest coherent amplitudes among the three target states, reaching $\alpha \approx 1.55$ at $g = 10$. The choice of target state thus depends on the experimental priority. If obtaining a larger coherent amplitude α is the primary objective, the scheme using $a^{\dagger 3}a^2S(\gamma)|Cat\rangle_{\pi,\alpha}$ (i.e., $|\psi_3\rangle$) exhibits the best performance; conversely, if a higher fidelity is required, adopting $a^{\dagger 3}aS(\gamma)|Cat\rangle_{\pi,\alpha}$ (i.e., $|\psi_2\rangle$) shows a significant advantage. Furthermore, $a^{\dagger 2}S(\gamma)|Cat\rangle_{\pi,\alpha}$ (i.e., $|\psi_1\rangle$) provides an excellent compromise that balances both the amplitude and high fidelity. These trends are clearly visible in the tables: $|\psi_2\rangle$ consistently gives the highest fidelity (especially for $r = 0.5$), $|\psi_3\rangle$ yields the largest α , and $|\psi_1\rangle$ sits in between with a balanced performance. Overall, the four-photon heralded state can be approximated with very high fidelity by any of these three target states, offering flexible trade-offs for different quantum information tasks.

D. Four-photon input and single-photon detection ($m = 4, n = 1$) and other cases

In the previous subsections we fixed the idler input to a single photon ($m = 1$) and varied the detected photon number $n = 2, 3, 4$. For $n = 2$, the output state approximates a squeezed odd cat state with amplitude $\alpha \sim \sqrt{3} \approx 1.732$ (see Sect. II A). For $n = 3$ and $n = 4$, the heralded states are even- and odd-parity Fock superpositions ($|0\rangle + |2\rangle + |4\rangle$ and $|1\rangle + |3\rangle + |5\rangle$), respectively, and analyzed in Sect. II B and Sect. II C.

A natural complementary question is whether one can instead inject more photons into the idler while detecting fewer photons at the output, and whether such a configuration can also generate large-amplitude SC states. Here we address this question by studying the case $m = 4$ (four photons at the idler input) and $n = 1$ (single-photon detection at the idler output). As will be shown, this configuration yields a SOSC state with coherent amplitude $\alpha \approx 2.24$, corresponding to an effective five-photon subtraction from the SV.

Substituting $m = 4, n = 1$ into the general formula Eq. (3) and using the SV input $|\phi\rangle = |\xi\rangle$, we obtain the unnormalized heralded state

$$|\Psi\rangle_{sv,4,1} = \sum_{k=0}^4 H(k, 4, 1)(a^\dagger)^{k-3}g^{-a^\dagger a}a^k|\xi\rangle \quad (30)$$

where the coefficient $H(k, 4, 1)$ is defined in Eq. (4). In this summation only the terms with $k = 3$ and $k = 4$ survive because the factorial $(k-3)!$ in the denominator is defined only for non-negative arguments. After evaluating the coefficients and using the properties of the squeezing operator, the state can be rewritten as a superposition of single-, three-, and five-photon added attenuated squeezed states:

$$|\Psi\rangle_{sv,4,1} = c'_1 a^\dagger |\frac{\xi}{g^2}\rangle + c'_3 a^{\dagger 3} |\frac{\xi}{g^2}\rangle + c'_5 a^{\dagger 5} |\frac{\xi}{g^2}\rangle, \quad (31)$$

where $|\xi/g^2\rangle$ denotes a SV state with the scaled squeezing parameter ξ/g^2 , and the coefficients c'_1, c'_3, c'_5 are given by

$$c'_1 = 3\xi^2 (g^{-1}c''_3 + c''_4), \quad (32a)$$

$$c'_3 = \frac{\xi^3}{g^2} (g^{-1}c''_3 + 6c''_4), \quad (32b)$$

$$c'_5 = \frac{\xi^4}{g^4} c''_4 \quad (32c)$$

with $c''_3 = H(3, 4, 1)$ and $c''_4 = H(4, 4, 1)$. In above derivation, we use

$$a|\xi\rangle = \xi a^\dagger |\xi\rangle, \quad (33)$$

$$a^2|\xi\rangle = \xi|\xi\rangle + \xi^2 a^{\dagger 2}|\xi\rangle. \quad (34)$$

A more compact representation that reveals the structure of photon subtraction is

$$|\Psi\rangle_{sv,4,1} = g^{-a^\dagger a} (c''_3 + c''_4 g a^\dagger a) a^3 |\xi\rangle. \quad (35)$$

This expression shows that the heralded state is a linear combination of 3-photon and 4-photon subtracted SV, followed by the noiseless attenuation operator $g^{-a^\dagger a}$ and an additional photon creation (embedded in the $a^\dagger a$ factor in the second term).

From the above equation one can deduce that the state $|\Psi\rangle_{sv,4,1}$ has odd parity and it can be approximated to a SOSC state with large coherent amplitude α . The reason is as follows. As we know, the 3-photon subtracted SV state $a^3|\xi\rangle$ can be well approximated by a SOSC state with coherent amplitude at most $\alpha \sim \sqrt{3} = 1.732$. However, in Eq. (35) the operator $a^\dagger a$ (multiplied by $c''_4 g$) acts on this state, and the photon number operator $a^\dagger a$ plays the role of amplifying the corresponding SC state. Furthermore, the squeezing operator $g^{-a^\dagger a}$ (or the final squeezing $S(\xi/g^2)$ in the normalized form) helps to pull apart the two peaks of the cat state. Hence, by properly adjusting the input signal squeezing parameter r , OPA

Table IV. Optimized parameters and fidelity for the approximation of $|\Psi\rangle_{sv,4,1}$ by the ideal SOSC state $|\Psi_\pi\rangle$ at fixed OPA gain $g = 1.5$. For each input squeezing r , coherent amplitude α , and the corresponding fidelity F are shown. All fidelity exceed 0.99, and the optimal α values are close to $\sqrt{5} \approx 2.236$.

| r | γ | α | F |
|-------|----------|----------|-------|
| 0.857 | 0.924 | 2.100 | 0.995 |
| 0.864 | 0.948 | 2.121 | 0.994 |
| 0.967 | 0.952 | 2.131 | 0.993 |
| 0.848 | 0.964 | 2.152 | 0.992 |
| 0.926 | 0.995 | 2.224 | 0.993 |

gain g , squeezing γ of the target SC state, one can realize the preparation of SOSC state with large amplitude ($\alpha \geq 2$) with high fidelity.

To demonstrate the capability of our $(m = 4, n = 1)$ configuration for generating large-amplitude SC states, we compare the heralded state $|\Psi\rangle_{sv,4,1}$ with the ideal SOSC state $|\Psi_\pi\rangle$. The Wigner functions of the two states are presented in Fig.9 (a) and (b), respectively, for OPA gain $g = 1.5$ and input squeezing $r = 1.0$. As shown in Fig.9(a) the heralded state exhibits a deep negative dip at the origin and two well-separated positive peaks, which are characteristic features of an odd SC state. The ideal target SOSC state with parameters $\alpha = 2.241$ and $\gamma = 1.0$ is displayed in Fig.9 (a), and its Wigner function shows remarkable similarity to that of the heralded state. The fidelity between the two states is calculated to be $F = 0.991$, confirming the excellent agreement. This high similarity is further corroborated by the spatial probability density distributions plotted in in Fig.9(c) (blue line for the heralded state, yellow line for the ideal target state), which closely match each other across the relevant spatial region.

Another significant aspect of the $(m = 4, n = 1)$ case is that it effectively approximates a five-photon subtraction from the squeezed vacuum state. For the $k = 5$ case, the $a^k|\xi\rangle$ can give well approximation to SOSC state $|\Psi_{sosc}\rangle$ with at most $\alpha \sim \sqrt{5} \approx 2.236$. Our numerical results, summarized in Table. IV for fixed OPA gain $g = 1.5$, and various input squeezing parameters r , confirm this behavior. For all considered values of r , the protocol consistently yields very high fidelities (all exceeding 0.99), and the optimal coherent amplitudes α are all close to $\sqrt{5}$. Specifically, the relative error between the optimized α and $\sqrt{5}$ is below 13.6% across the broad parameter ranges. These results demonstrate that the $(m = 4, n = 1)$ configuration provides a viable pathway for generating high-fidelity, large-amplitude SC states that are essential for fault-tolerant CV quantum information processing.

In the above subsections we have explicitly investigated the heralded states produced by the $(m = 1, n = 2)$, $(m = 1, n = 3)$, $(m = 1, n = 4)$ and $(m = 4, n = 1)$ configurations. Among these, the $(m = 1, n = 2)$ and

$(m = 4, n = 1)$ configurations effectively realize 3- and 5- photon subtraction from the input SV, respectively. Although not detailed in the preceding subsections, we have also examined the $(m = 3, n = 1)$ and $(m = 5, n = 1)$ cases; they yield 4- and 6-photon subtraction with fidelities ≥ 0.987 and ≥ 0.961 , respectively, over the full parameter ranges of g and r considered (see Table VI). In fact, we have systematically scanned all input-output pairs (m, n) with $0 \leq m, n \leq 7$ and identified the optimal configurations for each effective subtraction order k .

A central observation is that our protocol can effectively implement k -photon subtraction from the SV, but only for specific (m, n) pairs. Not every pair satisfying $m + n = k$ yields a SC state with amplitude $\alpha \approx \sqrt{k}$. Instead, by systematically optimizing the OPA gain g and the input squeezing parameter r , we have identified specific configurations where the heralded state approximates a certain type of squeezed SC state with extremely high fidelity and amplitude $\alpha \sim \sqrt{k}$. For example, the optimized $(m = 3, n = 1)$ and $(m = 4, n = 1)$ configurations realize 4- and 5-photon subtraction, respectively, yielding SESC and SOSC states with amplitudes $\alpha \approx \sqrt{4}$ and $\alpha \approx \sqrt{5}$. In contrast, the $(m = 1, n = 3)$ and $(m = 1, n = 4)$ configurations, despite having $m + n = 4$ and 5, give rise to qualitatively different states: even-parity Fock superpositions ($c_0|0\rangle + c_2|2\rangle + c_4|4\rangle$) and odd-parity Fock superpositions ($c_1|1\rangle + c_3|3\rangle + c_5|5\rangle$), rather than two-component SC states. This parity-dependent selection rule, which has no counterpart in conventional beam splitter based photon subtraction schemes, represents a new degree of control in OPA-based state engineering.

E. Quantum catalysis with $m = n$

In the above subsections we focused primarily on configurations with $m \neq n$, which effectively implement high-order photon subtraction from the SV with some parity-selected configurations. A distinct and equally interesting situation occurs when the number of input idler photons equals the number of detected photons, i.e., $m = n$. In this case the idler mode starts and ends in the same Fock state $|n\rangle$, the auxiliary mode is therefore restored after the interaction, acting as a quantum catalyst that enables a nontrivial transformation of the signal state without being consumed.

Setting $m = n$ in the general expression Eq. (10) and using the properties of the squeezing operator, we obtain a compact form for the heralded signal state:

$$|\Psi\rangle_{sv,n,n} = R_n(a^\dagger a) S\left(\frac{\xi}{g^2}\right) |0\rangle, \quad R_n(x) = \sum_{k=0}^n C_k x^k, \quad (36)$$

where coefficients $C_k = \alpha(\xi, g) H(k, n, n) g^k$. The state is therefore a superposition of photon-number-operator powers $(a^\dagger a)^k$ acting on a SV with scaled squeezing parameter ξ/g^2 . Due to parity conservation, it contains

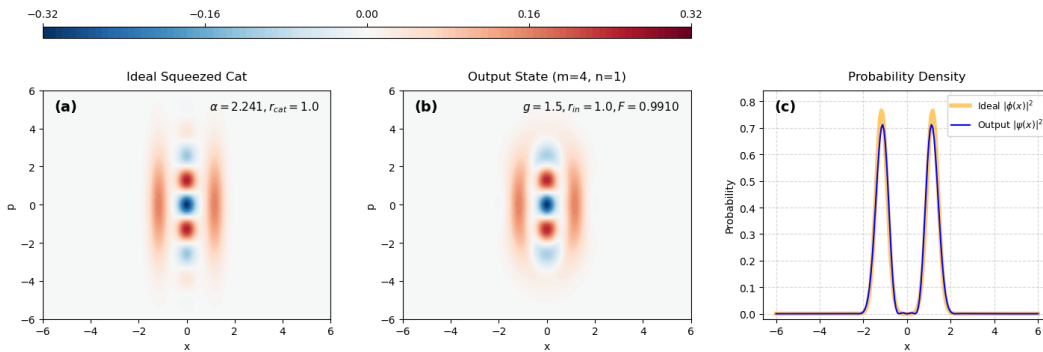


Figure 9. (a) Wigner function of the heralded state $|\Psi\rangle_{sv,4,1}$ with $g = 1.5$ and $r = 1.0$. (b) Wigner function of the ideal SOSOC target with $\alpha = 2.241$ and $\gamma = 1.0$. The fidelity between the two states is $F = 0.991$. (c) Spatial probability density distributions of the heralded state (blue curve) and the target state (yellow curve), confirming the high similarity in real space. The other parameters are the same as in Fig. 2.

only even Fock states (see the diagonal panels in Fig. 3). In this process, the auxiliary Fock state $|n\rangle$ is not changed by the successful heralding event, which is the defining feature of photon catalysis [43, 55].

For $n = 1$ this reduces to the single-photon catalysis studied in our previous work [45], where the output state approximates a small-amplitude SESC state. For $n = 2$, we obtain a new family of non-Gaussian states:

$$\begin{aligned} |\Psi\rangle_{sv,2,2} &\propto (C_0 + C_1 a^\dagger a + C_2 (a^\dagger a)^2) S(\xi/g^2) |0\rangle \\ &= S(\xi/g^2) [D_0|0\rangle + D_2|2\rangle + D_4|4\rangle], \end{aligned} \quad (37)$$

where the explicit expressions of coefficients D_0 , D_2 and D_4 can be obtained by straightforward algebra. This state contains only even Fock components and features a quadratic photon-number term ($a^\dagger a$), which is qualitatively different from states generated by conventional photon addition or subtraction. By tuning the OPA gain g and the input squeezing r , the relative weights $D_0 : D_2 : D_4$ can be varied continuously. Preliminary analysis shows that for appropriate parameters the $n = 2$ catalyzed state can offer a new resource for quantum metrology (see Fig. 12) and bosonic error correction.

Our state $|\Psi\rangle_{sv,2,2}$ can approximate a GKP state. GKP states encode qubits in CV modes and can protect against small quadrature shifts in phase space [47]. Ideal GKP states are superpositions of infinitely SV states and are unphysical due to infinite energy requirements. The preparation of optical GKP states, despite numerous theoretical and experimental efforts [62–66], continues to be a formidable task. In practice, finitely squeezed approximate GKP states are used. The logical basis states $|\tilde{0}\rangle$ and $|\tilde{1}\rangle$ in the position representation are given by [47]

$$\psi_{\tilde{0}}(x) = \frac{N_0}{(\pi\Delta^2)^{1/4}} \sum_{s=-\infty}^{+\infty} e^{-2\pi\Delta^2 s^2 - \frac{(x-2s\sqrt{\pi})^2}{2\Delta^2}}, \quad (38)$$

$$\psi_{\tilde{1}}(x) = \frac{N_1}{(\pi\Delta^2)^{1/4}} \sum_{s=-\infty}^{+\infty} e^{-\frac{1}{2}\pi\Delta^2(2s+1)^2 - \frac{[x-(2s+1)\sqrt{\pi}]^2}{2\Delta^2}}, \quad (39)$$

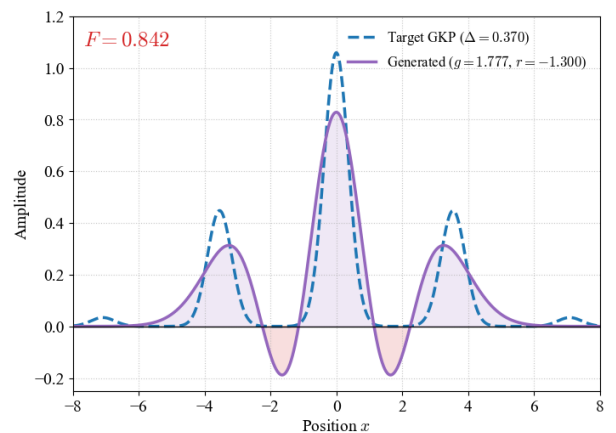


Figure 10. The wave functions of the target GKP state $\psi_{\tilde{0}}(x)$ (blue long dashed curve) with $\Delta = .37$ and our heralded state $|\Psi\rangle_{sv,2,2}$ (solid purple curve) with $g = 1.777$, $r = -1.300$. The fidelity between two states is 0.842. The other parameters are the same as in Fig. 2.

where $\Delta = e^{-r}$ characterizes the squeezing (standard deviation) and $N_{0,1}$ are normalization factors.

Both $\psi_{\tilde{0}}(x)$ and $\psi_{\tilde{1}}(x)$ are even function, matching the parity of our heralded state $|\Psi\rangle_{sv,2,2}$. As shown in Fig. 10, by optimizing the OPA gain g and input squeezing parameter r , we obtain a high fidelity of 0.842 between the ideal GKP state $|\tilde{0}\rangle$ and our state $|\Psi\rangle_{sv,2,2}$ for $g = 1.777$, $r = -1.300$, and $\Delta = 0.37$ (corresponding to 8.64 dB squeezing). For this $\Delta = 0.37$, the error probability of the approximate code word is on the order of 10^{-4} , which is acceptable for many quantum information tasks. The generation probability of our heralded state $|\Psi\rangle_{sv,2,2}$ for a successful single trial (see Sect. VI B) is 2.34×10^{-4} with above system parameters.

Our OPA-based heralding scheme unifies with quantum catalysis: for $m = n$ it enables higher-order catalysis (beyond single-photon level), producing squeezed low-dimensional Fock superpositions that are promising

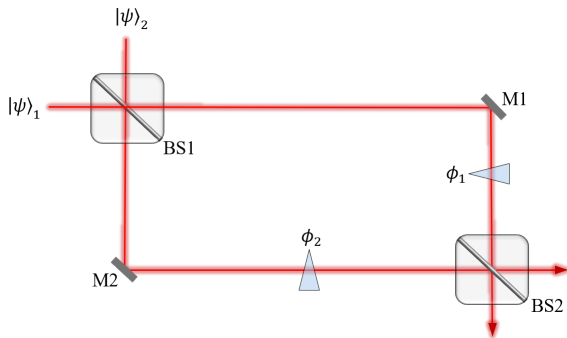


Figure 11. Mach-Zehnder interferometer setup for estimating an unknown phase difference. A heralded state, prepared according to our protocol, is sent into the interferometer. An unknown relative phase $\phi_1 - \phi_2$ is introduced by two linear phase shifters located in the two arms. This phase is imprinted onto the initial quantum state, and subsequent measurements at the output ports allow the phase to be estimated.

for low-photon metrology and GKP-state approximation [56]. This establishes the OPA as a versatile platform for non-Gaussian state engineering.

V. PHASE ESTIMATION WITH OUR HERALDED STATES

As mentioned above, the heralded non-Gaussian states produced by our protocol have potential applications in CV quantum information processing. As a concrete example, we demonstrate their advantages in phase estimation. The schematic of a Mach-Zehnder interferometer (MZI) for phase estimation is shown in Fig. 11. Two copies of our heralded state $|\Psi\rangle_{sv,n,m}$ are sent into the two input ports of the MZI, represented by annihilation (creation) operators a (a^\dagger) and b (b^\dagger) for the two arms, respectively. These operators obey the bosonic commutation relations $[a, a^\dagger] = [b, b^\dagger] = 1$, with all other commutators vanishing. The two phase shifters placed in the arms of the interferometer introduce an unknown relative phase shift $\phi = \phi_1 - \phi_2$. The unitary evolution imprinted on the input state is $U(\phi) = \exp(i\phi J)$, with the phase generator $J = (a^\dagger a - b^\dagger b)/2$, i.e., half the photon-number difference between the two arms. The encoded phase information is then read out via measurements at the output ports.

In quantum metrology, the sensitivity of estimating an unknown phase is characterized by quantum Fisher information (QFI). For a pure quantum state $|\Psi\rangle_0 = |\psi_1\rangle \otimes |\psi_2\rangle$, the QFI for estimating ϕ is defined as

$$\mathcal{F} = 4 \left[\langle \partial_\phi \Psi_0 | \partial_\phi \Psi_0 \rangle - |\langle \Psi_0 | \partial_\phi \Psi_0 \rangle|^2 \right]. \quad (40)$$

For an unbiased estimation, the phase uncertainty is

bound by the quantum Cramér-Rao bound

$$\Delta^2 \phi \geq \frac{1}{N_1 \mathcal{F}}, \quad (41)$$

where N_1 is the total number of measurements and in the following content we take $N_1 = 1$. A higher QFI means a better estimation precision. For the unitary evolution $U(\phi) = \exp(i\phi J)$ applied to the input state $|\Psi_0\rangle$, the QFI reduces to [18, 57]

$$\mathcal{F} = 4 \langle \Psi_0 | \Delta^2 \mathcal{H} | \Psi_0 \rangle, \quad (42)$$

where $\mathcal{H} = i(\partial_\phi U^\dagger)U$ and $\Delta^2 \mathcal{H} = (\mathcal{H} - \langle \mathcal{H} \rangle)^2$. For a pure, path-symmetric input state $|\Psi_0\rangle = |\psi_1\rangle \otimes |\psi_1\rangle$ (two identical copies of the heralded state entering the two ports) with equal mean photon numbers in the two arms, the QFI simplifies to [19, 21]

$$\mathcal{F} = 2\Delta^2(n_a), \quad (43)$$

where $n_a = a^\dagger a$. This shows that the QFI is determined solely by the photon-number variance of the heralded state.

Previous studies have shown that using coherent and NOON states as input resources [58], the standard quantum limit (SQL) $\propto N$ and Heisenberg limit (HL) $\propto N^2$ can be reached, where N is the total average photon number of the two arms. For a SV state with squeezing parameter r , the QFI is $\mathcal{F}_{sv} = N^2 + 2N$, which can exceed the HL [19]. We now examine whether our heralded states generated from SV via the OPA can outperform the SV itself. In this work, we define the HL limit as $\mathcal{F}_{HL} = N^2$ (the scaling achieved by NOON states).

Based on Eq. (43), we can evaluate the QFI analytically for the heralded output states $|\Psi\rangle_{sv,m,n}$ by different configurations (m, n). As specific examples, we choose eight configurations: $(m = 1, n = 1)$ to $(1, 4)$, $(m = 3, n = 1)$, $(m = 2, n = 2)$, $(m = 3, n = 3)$ and $(m = 4, n = 1)$. The numerical results are shown in Fig. 12.

In Fig. 12 (a), we plot the QFI of these states as a function of the squeezing parameter (ranging from 0 to 3), which determines the average photon number. The OPA gain is fixed to $g = 1.04$. For large photon number, the QFI values of the heralded states are all higher than the SQL and the HL, especially for the $(m = 1, n = 4)$, $(m = 4, n = 1)$, $(m = 1, n = 3)$ and $(m = 3, n = 1)$ configurations. In the low-photon-number regimes, however, the QFI of the above configurations (except $(m = 1, n = 1)$, $(m = 1, n = 2)$, $(m = 3, n = 1)$) are lower than the HL, while (except $(m = 1, n = 1)$, $(m = 1, n = 2)$, $(m = 3, n = 1)$) exceed the HL, as shown in the inset of Fig. 12 (a). Despite their limited performance at large photon numbers, the catalyzed states with $m = n$ achieve super-Heisenberg scaling in the low-photon-number regime, which is particularly relevant for loss-sensitive or low-flux metrology. The degradation below the Heisenberg limit at higher photon numbers is caused by the intrinsic Fock cutoff at

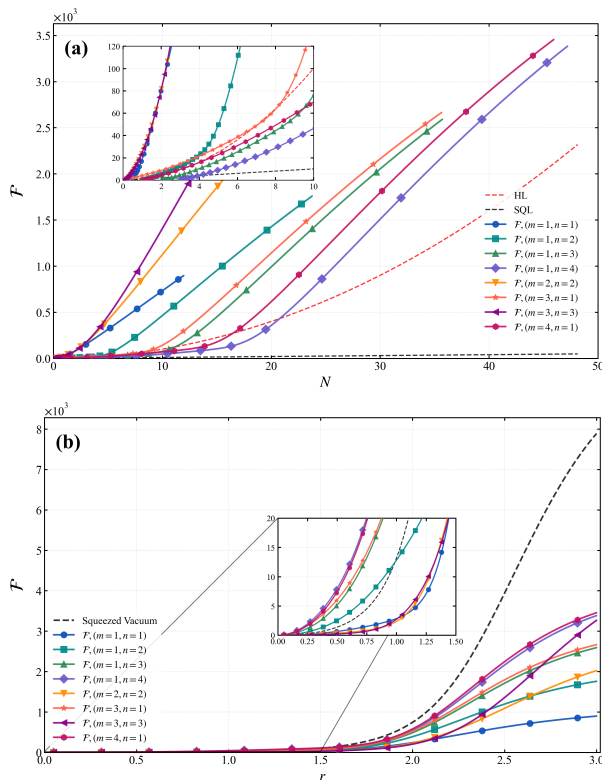


Figure 12. Quantum Fisher information (QFI) \mathcal{F} plotted as a function of the average photon number N and squeezing parameter in (a) and (b), respectively, with different photon heralded states corresponding to some configurations (m, n) . Here, SQL and HL denote the standard quantum limit (SQL) N and Heisenberg limit (HL) N^2 , and the OPA gain fixed to $g = 1.04$. The other parameters are the same as in Fig. 2.

$2n$ photons, which bounds the mean photon number and saturates the photon-number variance.

In Fig. 12 (b), we present the QFI as a function of the squeezing parameter r for the same configurations, again with $g = 1.04$, and compare them with the SV reference. In weak squeezing input regime (see the inset), all configurations except $(m = 1, n = 1)$ yield a better phase estimation performance than the SV. In the moderate-squeezing regime, the QFI of $(m = 1, n = 4)$, $(m = 4, n = 1)$ and $(m = 3, n = 1)$ remains larger than that of the SV. However, in the strong-squeezing regime, the scaling of the QFI for most configurations approaches the SQL but remains inferior to the HL.

One can understand the mechanism of enhanced phase estimation with our heralded states as follows. For our pure and separable initial states, the QFI can be expressed in terms of the Mandel $\mathcal{Q} = [\Delta^2(n_a) - \langle n_a \rangle] / \langle n_a \rangle$ factor as

$$\mathcal{F} = N(1 + \mathcal{Q}). \quad (44)$$

Our calculations show that for the heralded states considered, the Mandel \mathcal{Q} factor is approximately proportional to the average photon number. Consequently, the

proportionality constant, which is larger than unity, allows the QFI to numerically exceed the HL in the large-photon-number limit, while still maintaining the same quadratic scaling.

From the above discussion we can conclude that the phase estimation precision using our heralded states can achieve excellent performance and even surpass the HL over a wide range of input squeezing parameters, provided the OPA gain g is chosen appropriately. Among the states considered, the $(m = 1, n = 4)$, $(m = 4, n = 1)$ and $(m = 1, n = 3)$ configurations, which possess high complexity and negativity, give the best performance. Furthermore, for phase estimation in the weak-squeezing regime, the heralded states produced by our protocol are preferable to the SV itself.

VI. PRACTICAL CONSIDERATIONS

In this section, we analyze the experimental feasibility of our heralded non-Gaussian state generation scheme. We consider two key practical aspects: the detrimental effects of photon loss and dephasing, and the overall success probabilities for different parameter configurations, including the use of high-repetition-rate laser sources to overcome low single-trial success probabilities.

A. Photon loss and dephasing

In any realistic optical implementation, quantum states are subject to decoherence due to interaction with the environment. For bosonic modes, the dominant imperfections are single-photon loss and dephasing. The dynamics of the system under these noise channels can be described by the master equation

$$\frac{d\rho(t)}{dt} = (\kappa \mathcal{D}[a] \rho + \kappa_\phi \mathcal{D}[a^\dagger a]) \rho(t) \quad (45)$$

where κ and κ_ϕ are the photon loss and dephasing rates, respectively, and $\mathcal{D}[A] \rho \equiv 2A\rho A^\dagger - A^\dagger A \rho - \rho A^\dagger A$ is the Lindblad dissipator. Note that loss and dephasing errors are generated by the jump operator a and $a^\dagger a$ respectively. We say that a system state is loss-dominated (dephasing-dominated) if $\kappa \gg \kappa_\phi$ ($\kappa_\phi \gg \kappa$).

To assess the robustness of our scheme against environmental decoherence, we numerically simulate the effects of single-photon loss and dephasing on the fidelity of the heralded states. The dynamics is governed by the master equation in Eq. (45). For the configurations $(m = 1, n = 2)$ and $(m = 4, n = 1)$, which produce approximated SOSC states with amplitude $\alpha \sim 1.73$ and $\alpha \sim 2.237$, respectively, we evaluate the fidelity with respect to the ideal target state $|\Psi_{sosc}\rangle$, with fixed squeezing $r = 1.0$ and OPA gain $g = 1.5$.

Figure 13 presents the optimal fidelity as a function of the target coherent amplitude α for different noise scenarios: pure photon loss ($\kappa_\phi = 0$), loss-dominated case

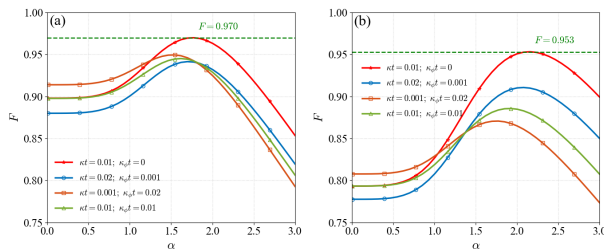


Figure 13. Fidelity of heralded states $|\Psi\rangle_{sv,1,2}$ (a) and $|\Psi\rangle_{sv,4,1}$ (b) with respect to the ideal SOSC state $|\Psi_{sosc}\rangle$ under photon loss and dephasing. OPA gain and input SV's squeezing are set to $g = 1.5$ and $r = 1.0$. The other parameters are the same as in Fig. 2.

($\kappa/\kappa_\phi = 20$), dephasing-dominated case ($\kappa_\phi/\kappa = 20$) and equivalent rates ($\kappa = \kappa_\phi$). The fidelity of ($m = 4$, $n = 1$) configuration more sensitive to losses than that of the ($m = 1$, $n = 2$) case. For the pure photon loss with $\kappa t = 0.01$, the optimal overlap remains above 0.95 in both configurations, with optimal target parameters $\alpha = 1.84$, $\gamma = 0.703$ for ($m = 1$, $n = 2$) and $\alpha = 2.16$, $\gamma = 0.966$ for ($m = 4$, $n = 1$) (see blue solid curves in Fig.13 (a) and (b), respectively.)

Comparing the photon-loss dominated ($\kappa/\kappa_\phi = 20$) and dephasing-dominated ($\kappa_\phi/\kappa = 20$) cases reveals different effects. For ($m = 1$, $n = 2$) configuration, the optimal fidelity in dephasing-dominated case is higher than that photon loss-dominated case, while the former also yields a larger coherent amplitude α (see blue and orange curves in Fig.13 (a)). In contrast, for ($m = 4$, $n = 1$) configuration, both the optical fidelity and the corresponding coherent amplitude of target SOSC state are lower in the dephasing-dominated than in the photon loss-dominated case. Furthermore, we observe that the equal amounts of photon loss and dephasing ($\kappa = \kappa_\phi$) give better performance than either the photon loss-dominated or dephasing-dominated case for both configurations. As we can see, dephasing significantly diminishes the interference fringes of the quantum state in the phase space, leading to a decrease in the optimal fidelity between our heralded state and target states.

To further illustrate the effects of pure photon loss on the optimal fidelity between our heralded states—which effectively realize three-, four- and five-photon subtraction—and on different types of squeezed SC states, we show in Fig. 14 the changes of the most optimized fidelity F , negativity N and complexity \mathcal{C} of our heralded states $|\Psi\rangle_{sv,m,n}$ for ($m = 1$, $n = 2$), ($m = 3$, $n = 1$) and ($m = 4$, $n = 1$) as functions of the photon loss rate κt .

As can be seen, the optimal fidelity F for all three configurations decreases with increasing κt . The most optimized fidelities— $F = 0.997$ (for (1, 2) with $\alpha_{opt} = 1.795$, $\gamma_{opt} = 0.706$), $F = 0.984$ (for (3, 1) with $\alpha_{opt} = 1.9$, $\gamma_{opt} = 0.979$), and $F = 0.991$ (for (4, 1) with $\alpha_{opt} = 2.2$, $\gamma_{opt} = 0.986$)—remain high ($F \geq 0.9$) in the regimes $\kappa t \leq 0.038$, $\kappa t \leq 0.031$ and $\kappa t \leq 0.025$, respectively.

These high fidelities drop from ≥ 0.98 at zero loss to approximately 0.766, 0.759 and 0.700 at $\kappa t = 0.1$ (i.e., 10% single-photon loss).

The negativity \mathcal{N} and complexity \mathcal{C} of our heralded states also decreases with increasing κt , eventually reaching their minimum values 0 and 1, respectively. Interestingly, even at 10% single photon loss ($\kappa t = 0.1$), the negativity and complexity of these states are not small. For $\kappa t \gtrsim 0.33$, the negativity \mathcal{N} becomes zero while the complexity \mathcal{C} remains larger than 1. For our heralded states, \mathcal{C} does not become exactly 1 even when the photon loss rate is as high as $\kappa t = 1$ (see Fig. 14 (a) and (b)). This indicates that the negativity \mathcal{N} and complexity \mathcal{C} of our heralded states have excellent robustness against the single-photon loss, especially for those states that initially possess high complexity and negativity.

Overall, these results demonstrate that our protocol is compatible with state-of-the-art experimental conditions: moderate single-photon loss or dephasing alone preserves high fidelities, confirming the practical feasibility of the scheme. Nevertheless, when photon loss and dephasing are present at comparable rates, the fidelity can be significantly reduced, while negativity \mathcal{N} and complexity \mathcal{C} remain with considerable values. This resilience indicates that our states retain useful quantum resources under realistic loss, with potential advantages in fault-tolerant quantum computing [23, 24, 59], lossy quantum metrology [21, 60], and state certification [61].

B. Success probability

The total probability per trial for successfully generating a heralded non-Gaussian state in our scheme can be expressed as

$$P_{trial} = \eta_{det} \times P_{Fock}(m, \tau) \times P_{sv}(r, g, m, n) \quad (46)$$

where $P_{Fock}(m, g')$ is the probability to generate m -photon Fock state at the idler input via spontaneous parametric down-conversion (SPDC) using a pump with gain parameter g' ; $P_{sv}(r, r, g, n)$ is the conditional heralding probability for the OPA stage, i.e., the probability that the idler output contains exactly n -photons given an input m -photon Fock state and a SV (squeezing parameter r) in the signal mode; η_{det} is the system detection efficiency of the PNRD, which includes intrinsic quantum efficiency, coupling losses, and filtering losses.

The m -photon Fock state can be prepared by seeding an SPDC source (OPA) with vacuum and heralding on the detection of m photons. The SPDC process is described by the same two-mode squeezing unitary as the OPA [see Eq. (1)], so that the m -photon state can be expressed as

$$|m\rangle_{Fock} = {}_b\langle m| (\mathbb{I} \otimes \Pi_n) S(\tau') (|0\rangle_a \otimes |0\rangle_b). \quad (47)$$

The preparation probability $P_{Fock}(m, g')$ is given by the norm square of this unnormalized state. For the parameters used in this work, we take $g' = 1.0483$ and

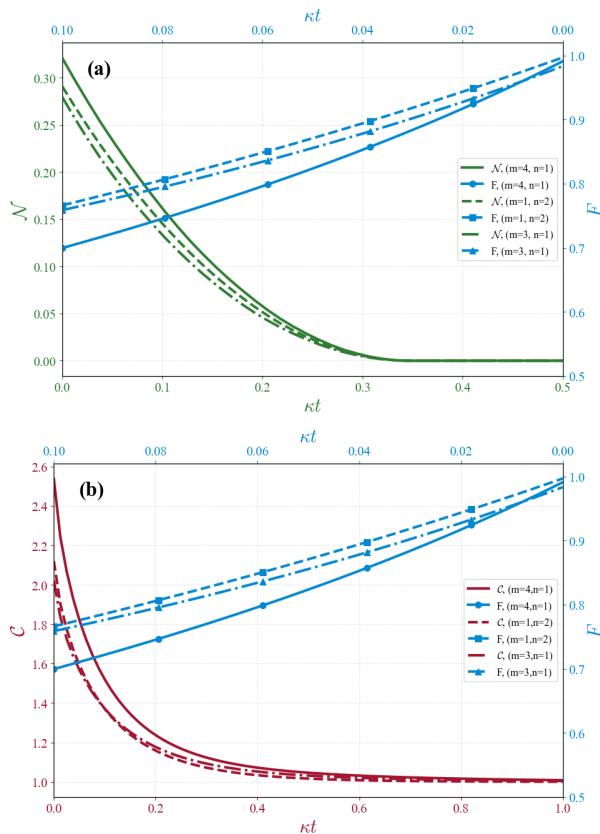


Figure 14. Changes of the fidelity F , negativity \mathcal{N} and complexity \mathcal{C} of our heralded states $|\Psi\rangle_{sv,m,n}$ with $(m=1, n=2)$, $(m=3, n=1)$ and $(m=4, n=1)$ configurations vs photon loss rate κt . Here, the most optimized fidelity for different configurations as follow: (i) $(m=1, n=2)$ configuration, $\alpha_{opt} = 1.795$, $\gamma_{opt} = 0.706$, $F = 0.997$; (ii) $(m=3, n=1)$ configuration, $\alpha_{opt} = 1.9$, $\gamma_{opt} = 0.979$, $F = 0.984$; (iii) $(m=4, n=1)$ configuration, $\alpha_{opt} = 2.2$, $\gamma_{opt} = 0.986$, $F = 0.991$. The other parameters are the same as in Fig. 2.

compute the relevant probabilities. Modern superconducting nanowire single-photon detectors can be operated in a photon-number-resolving mode with high efficiency [62]. We adopt a conservative value $\eta_{det} = 0.9$ (90%) which is routinely achieved in state-of-the-art experiments [63, 64].

Table IX lists the success probabilities for various (m, n) combinations, with input squeezing $r = 1.0$ (≈ 8.69 dB) and OPA gain $g = 1.5$. P_{Fock} and P_{sv} are obtained from numerical calculations; P_{trial} is computed as their product times η_{det} .

For the $(m=1, n=2)$ configuration, which produces a high-fidelity SOSC state with amplitude $\alpha \approx 1.73$, the total trial probability is $P_{trial} \approx 1.4 \times 10^{-2} = 1.4\%$. This is remarkably high for a heralded non-Gaussian state source and is directly comparable to the success rates reported in state-of-the-art GPS experiments [32, 34]. The dominant contribution comes from $P_{sv} = 1.56 \times 10^{-1}$,

Table V. Success probabilities of our heralded state with (m, n) . Parameters: $r = 1.0$, $g' = 1.0483$, $g = 1.5$ and $\eta_{det} = 0.9$.

| (m, n) | $P_{Fock}(m, g')$ | $P_{sv}(r, g, m, n)$ | P_{trial} |
|----------|-----------------------|-----------------------|-----------------------|
| (1, 1) | | 1.58×10^{-1} | 1.16×10^{-2} |
| (1, 2) | 8.19×10^{-2} | 1.56×10^{-1} | 1.15×10^{-2} |
| (1, 3) | | 1.29×10^{-1} | 9.57×10^{-3} |
| (1, 4) | | 1.00×10^{-1} | 7.42×10^{-3} |
| (2, 2) | 7.38×10^{-3} | 8.11×10^{-2} | 5.38×10^{-4} |
| (3, 1) | 6.64×10^{-4} | 3.95×10^{-2} | 2.36×10^{-5} |
| (4, 1) | 5.98×10^{-5} | 1.15×10^{-2} | 6.20×10^{-7} |
| (5, 1) | 5.38×10^{-6} | 1.15×10^{-2} | 5.58×10^{-8} |
| (5, 2) | | 6.17×10^{-3} | 2.99×10^{-8} |

which is favorable because $n = 2$ detection is efficient and $m = 1$ (single photon) can be generated near-deterministically.

For the $(m=4, n=1)$ configuration (amplitude $\alpha \sim \sqrt{5} \approx 2.236$), $P_{trial} \approx 6.20 \times 10^{-7}$. This low value is primarily due to the small $P_{Fock}(4, \tau) = 5.98 \times 10^{-5}$, reflecting the difficulty of generating a four-photon Fock state in a single trial with SPDC process. This obstacle could, in principle, be overcome by employing alternative, near-deterministic methods for preparing higher-order Fock states, such as those demonstrated in cavity and circuit QED systems [9, 65, 66]. In particular, the conditional measurement protocol of Zhang & Jing [9], which is conceptually similar to our heralding approach, can generate Fock states $|m\rangle$ with fidelity exceeding 99% in less than 30 measurement cycles, even for $n \sim 10$. Integrating such a high-fidelity, efficient source of m -photon Fock states with our OPA scheme would effectively eliminate the P_{Fock} factor, potentially boosting P_{trial} by several orders of magnitude. Nevertheless, with current SPDC technology, low single-trial probabilities may still raise concerns about experimental feasibility; it is comparable to or even higher than the heralding probabilities reported in successful multiphoton state engineering experiments. For instance, in the experimental preparation of three-photon-added coherent states, Fadrić et al. achieved heralding probabilities on the order of 10^{-9} for similar multiphoton operations [7].

Low single-trial probabilities can be effectively overcome by operating the pump laser at a high repetition rate. A standard 80 MHz repetition rate yields $R_{herald} = P_{trial} \times f_{rep} = 6.20 \times 80 \times 10^6 \approx 50$ Hz (50 states per second), permitting accumulation of millions of heralded states per day, sufficient for high-fidelity tomography and quantum information tasks. State-of-the-art laser systems can achieve repetition rates in the GHz regime (e.g., 1 GHz to 50 GHz) [64, 67, 68] even in terahertz (THz) [64] regimes, the rate can be boosted to thousands of hertz. For the $(m=1, n=2)$ case, under the 1.55- μ m-driven difference-frequency generation with a 32 MHz repetition rate which can be operated in the regime of OPA [69], it can give approximately 4.76×10^5 state per second, which is exceptionally high and exceeds the

rates reported in recent experimental demonstrations of SC state generation [70].

Thus, despite varying single-trial probabilities, the combination of heralded operation, high-repetition-rate pumping, and efficient PNRDs [71] makes all configurations experimentally feasible. Our OPA-based scheme is well within reach of current optical quantum technologies.

VII. CONCLUSION

In this study, we have proposed and analyzed a multiphoton heralding scheme based on an OPA that generates non-Gaussian states of light with controllable higher-Fock components from a SV input. In contrast to our previous work [45], which considered only the (1,1) case, here we uncover a parity-dependent selection rule that determines whether a heralded state approximates a SC state or a multi-Fock superposition. Such a selection rule does not arise in conventional k -photon subtraction schemes based on a BS. In our OPA scheme, it emerges naturally and provides an additional degree of control. By varying the input–output photon pair (m, n) , the OPA gain g , and the input squeezing r , one can steer the output state between SC-like and multi-Fock superpositions. We have found that systematic optimization of the g and r yields a certain type of squeezed SC state with extremely high fidelity and amplitude at most $\alpha \approx \sqrt{k}$ for some specific configurations satisfying $m + n = k$. Table VI summarizes the optimized configurations that effectively realize k -photon subtraction for $k = 1$ to 7, along with the optimized corresponding target parameters (squeezing parameter γ , coherent amplitude α , and fidelity F) and the type of non-Gaussian state produced.

Beyond state engineering, we have systematically characterized the non-classicality and structural richness of our heralded states using Wigner negativity \mathcal{N} and complexity \mathcal{C} . The results show that states with higher \mathcal{N} and \mathcal{C} (e.g., $(m = 1, n = 4)$ and $(m = 4, n = 1)$) exhibit superior performance in phase estimation, achieving QFI that surpasses both the SQL and the HL (defined as N^2) over a wide range of parameters. Moreover, these states demonstrate remarkable robustness against photon loss:

even when \mathcal{N} vanishes under strong loss, \mathcal{C} persists, highlighting the resilience of their structural complexity.

Regarding experimental feasibility, the total success probability for the high-performance $(m = 1, n = 2)$ configuration reaches 1.15% per trial, while the large-amplitude $(m = 4, n = 1)$ configuration has a single-trial probability on the order of 10^{-7} . These probabilities are comparable to those of other heralded non-Gaussian state schemes (e.g., multi-photon-added coherent states [7] and cluster states [72]). Although low at first glance, such probabilities can be effectively overcome by operating the pump laser at a high repetition rate transforming per-trial probabilities into absolute heralding rates. This places the predicted performance of our protocol on par with state-of-the-art experimental demonstrations. Nevertheless, practical implementation demands high phase stability in the idler interferometer, low photon loss, and high detector efficiency to maintain output fidelity. With continued progress in high-repetition-rate lasers, low-loss integrated photonics, and high-efficiency superconducting detectors, our scheme provides a scalable and viable pathway for advanced quantum state engineering.

Our protocol thus provides a flexible and integrated platform for engineering higher-order photon subtraction and generating a rich family of non-Gaussian states—ranging from squeezed SC states to even- and odd-parity Fock superpositions. In particular, the catalyzed state with $m = n = 2$ is shown to approximate a finite-energy GKP codeword with a fidelity of 0.842 (see Fig. 10), demonstrating the potential of our scheme for generating bosonic error-correction resources. This work establishes the OPA as a versatile, reconfigurable tool for non-Gaussian state engineering, and opens new directions for exploring the interplay between structural complexity, quantum metrology, and fault-tolerant quantum information processing.

ACKNOWLEDGMENTS

This study was supported by the National Natural Science Foundation of China (No. 12365005).

-
- [1] S. L. Braunstein and P. van Loock, *Rev. Mod. Phys.* **77**, 513 (2005).
 - [2] M. Walschaers, V. Parigi, and N. Treps, *PRX Quantum* **1**, 020305 (2020).
 - [3] L. Lachman and R. Filip, *Prog. Quantum Electron.* **83**, 100395 (2022).
 - [4] M. Walschaers, *PRX Quantum* **2**, 030204 (2021).
 - [5] P. Zapletal, A. Nunnenkamp, and M. Brunelli, *PRX Quantum* **3**, 010301 (2022).
 - [6] M. S. Winnel, J. J. Guanzon, D. Singh, and T. C. Ralph, *Phys. Rev. Lett.* **132**, 230602 (2024).
 - [7] J. FadrnÅœ, M. Neset, M. Bielak, M. JeÅŸek, J. BÅlek, and J. FiurÅŸek, *npj Quantum Inf.* **10**, 89 (2024).
 - [8] W. Wang, L. Hu, Y. Xu, K. Liu, Y. Ma, S.-B. Zheng, R. Vijay, Y. P. Song, L.-M. Duan, and L. Sun, *Phys. Rev. Lett.* **118**, 223604 (2017).
 - [9] C.-y. Zhang and J. Jing, *Phys. Rev. A* **110**, 042421 (2024).
 - [10] K. Miyata, H. Ogawa, P. Marek, R. Filip, H. Yonezawa, J.-i. Yoshikawa, and A. Furusawa, *Phys. Rev. A* **93**, 022301 (2016).
 - [11] Y. Zheng, O. Hahn, P. Stadler, P. Holmval, F. Qui-

Table VI. The realization of effective k -photon (up to 7-photon) subtraction with our protocol.

| k | (m, n) | SC type | κ_ϕ | α | F | Realization with BS scheme (Exps) |
|-----|------------------|---------|-----------------|----------------|-------------------|-----------------------------------|
| 1 | (1, 0) or (0, 1) | odd | 0.30 ± 0.06 | 0.9 ± 0.1 | 0.998 ± 0.001 | Ref. [26, 32] |
| 2 | (1, 1) | even | 0.59 ± 0.07 | 1.4 ± 0.1 | 0.997 ± 0.001 | Ref. [27] |
| 3 | (1, 2) | odd | 0.45 ± 0.15 | 1.7 ± 0.1 | 0.998 ± 0.001 | Ref. [28, 73] |
| 4 | (3, 1) | even | 1.07 ± 0.07 | 2.0 ± 0.1 | 0.970 ± 0.010 | Ref. [74] |
| 5 | (4, 1) | odd | 1.15 ± 0.15 | 2.2 ± 0.1 | 0.993 ± 0.002 | — ^a |
| 6 | (5, 1) | even | 1.24 ± 0.04 | 2.45 ± 0.1 | 0.920 ± 0.010 | — |
| 7 | (5, 2) | odd | 0.95 ± 0.04 | 2.6 ± 0.1 | 0.979 ± 0.005 | — |

^a No experiment reported to date

- jandría, A. Ferraro, and G. Ferrini, *PRX Quantum* **2**, 010327 (2021).
- [12] T. Yoshida, D. Okuno, T. Kashiwazaki, T. Umeki, S. Miki, F. China, M. Yabuno, H. Terai, and S. Takeda, *PRX Quantum* **6**, 010311 (2025).
- [13] A. L. Grimsmo and S. Puri, *PRX Quantum* **2**, 020101 (2021).
- [14] S. B. Korolev, E. N. Bashmakova, and T. Y. Golubeva, *Quantum Inf. Process.* **23**, 354 (2024).
- [15] E. Knill and R. Laflamme, *Phys. Rev. A* **55**, 900 (1997).
- [16] K. Fukui, A. Tomita, A. Okamoto, and K. Fujii, *Phys. Rev. X* **8**, 021054 (2018).
- [17] T. C. Ralph, A. Gilchrist, G. J. Milburn, W. J. Munro, and S. Glancy, *Phys. Rev. A* **68**, 042319 (2003).
- [18] J. Liu, X.-X. Jing, and X. Wang, *Sci. Rep.* **5**, 8565 (2015).
- [19] J. Sahota and N. Quesada, *Phys. Rev. A* **91**, 013808 (2015).
- [20] X.-X. Zhang, Y.-X. Yang, and X.-B. Wang, *Phys. Rev. A* **88**, 013838 (2013).
- [21] P. A. Knott, T. J. Proctor, A. J. Hayes, J. P. Cooling, and J. A. Dunningham, *Phys. Rev. A* **93**, 033859 (2016).
- [22] M. H. Michael, M. Silveri, R. T. Brierley, V. V. Albert, J. Salmilehto, L. Jiang, and S. M. Girvin, *Phys. Rev. X* **6**, 031006 (2016).
- [23] Y. Zeng, F. Quijandría, C. Gneiting, and F. Nori, *Phys. Rev. Lett.* **136**, 190602 (2026).
- [24] Q. Xu, G. Zheng, Y.-X. Wang, P. Zoller, A. A. Clerk, and L. Jiang, *npj Quantum Inf.* **9**, 78 (2023).
- [25] M. Dakna, T. Anhut, T. Opatrny, L. Knöll, and D.-G. Welsch, *Phys. Rev. A* **55**, 3184 (1997).
- [26] A. Ourjoumtsev, R. Tualle-Brouri, J. Laurat, and P. Grangier, *Science* **312**, 83 (2006).
- [27] H. Takahashi, K. Wakui, S. Suzuki, M. Takeoka, K. Hayasaka, A. Furusawa, and M. Sasaki, *Phys. Rev. Lett.* **101**, 233605 (2008).
- [28] T. Gerrits, S. Glancy, T. S. Clement, B. Calkins, A. E. Lita, A. J. Miller, A. L. Migdall, S. W. Nam, R. P. Mirin, and E. Knill, *Phys. Rev. A* **82**, 031802(R) (2010).
- [29] V. Parigi, A. Zavatta, M. Kim, and M. Bellini, *Science* **317**, 1890 (2007).
- [30] A. Ourjoumtsev, H. Jeong, R. Tualle-Brouri, and P. Grangier, *Nature* **448**, 784 (2007).
- [31] K. Wakui, H. Takahashi, A. Furusawa, and M. Sasaki, *Opt. Express* **15**, 3568 (2007).
- [32] K. Takase *et al.*, *Opt. Express* **30**, 14161 (2022).
- [33] M. Javid, I. Noreen, R. Iqbal, and M. Idrees, *Opt. Quantum Electron.* **58**, 218 (2026).
- [34] K. Takase, J.-i. Yoshikawa, W. Asavanant, M. Endo, and A. Furusawa, *Phys. Rev. A* **103**, 013710 (2021).
- [35] H. Tomoda, A. Machinaga, K. Takase, J. Harada, T. Kashiwazaki, T. Umeki, S. Miki, F. China, M. Yabuno, H. Terai, D. Okuno, and S. Takeda, *Phys. Rev. A* **110**, 033717 (2024).
- [36] X.-X. Yao and Y. Turek, *npj Quantum Information* (2026).
- [37] Q. Hu, T. Yusufu, and Y. Turek, *Phys. Rev. A* **105**, 022608 (2022).
- [38] X.-X. Yao and Y. Turek, *Quantum Sci. Technol.* **11**, 025038 (2026).
- [39] J. Fiurášek, S. Grebien, and R. Schnabel, *Phys. Rev. A* **111**, 043704 (2025).
- [40] S. Grebien, J. Göttlich, B. Hage, J. Fiurášek, and R. Schnabel, *Phys. Rev. Lett.* **129**, 273604 (2022).
- [41] Y. Kurochkin, A. S. Prasad, and A. I. Lvovsky, *Phys. Rev. Lett.* **112**, 070402 (2014).
- [42] A. I. Lvovsky and J. Mlynek, *Phys. Rev. Lett.* **88**, 250401 (2002).
- [43] A. Aralov, E. Gillet, V. Nguyen, A. Cosentino, M. Walschaers, and M. Frigerio, *PRX Quantum* **7**, 020323 (2026).
- [44] S. U. Shringarpure and J. D. Franson, *Phys. Rev. A* **100**, 043802 (2019).
- [45] X.-X. Yao, B. Zhang, and Y. Turek, *Phys. Rev. A* **113**, 033712 (2026).
- [46] J. Johansson, P. Nation, and F. Nori, *Comput. Phys. Commun.* **184**, 1234 (2013).
- [47] D. Gottesman, A. Kitaev, and J. Preskill, *Phys. Rev. A* **64**, 012310 (2001).
- [48] O. Erkilic, A. Das, B. Shajilal, P. K. Lam, T. C. Ralph, and S. M. Assad, “A unified optical platform for non-gaussian and fault-tolerant Gottesman-Kitaev-Preskill states,” (2025), arXiv:2512.02607 [quant-ph].
- [49] R. A. Brewster, I. C. Nodurft, T. B. Pittman, and J. D. Franson, *Phys. Rev. A* **96**, 042307 (2017).
- [50] A. Kenfack and K. Życzkowski, *J Opt B Quantum Semi-classical Opt* **6**, 396 (2004).
- [51] S. Tang, F. Albarelli, Y. Zhang, S. Luo, and M. G. A. Paris, *Quantum Sci. Technol.* **10**, 045047 (2025).
- [52] P. Marek, H. Jeong, and M. S. Kim, *Phys. Rev. A* **78**, 063811 (2008).
- [53] A. L. Grimsmo, J. Combes, and B. Q. Baragiola, *Phys. Rev. X* **10**, 011058 (2020).
- [54] D. S. Schlegel, F. Minganti, and V. Savona, *Phys. Rev. A* **106**, 022431 (2022).
- [55] R. J. Birrittella, M. E. Baz, and C. C. Gerry, *J. Opt. Soc. Am. B* **35**, 1514 (2018).
- [56] D. Su, C. R. Myers, and K. K. Sabapathy, *Phys. Rev. A*

- 100**, 052301 (2019).
- [57] J. Liu, M. Zhang, H. Chen, L. Wang, and H. Yuan, *Adv. Quantum Technol.* **5**, 2100080 (2022).
- [58] A. N. Boto, P. Kok, D. S. Abrams, S. L. Braunstein, C. P. Williams, and J. P. Dowling, *Phys. Rev. Lett.* **85**, 2733 (2000).
- [59] Y.-H. Chen, W. Qin, R. Stassi, X. Wang, and F. Nori, *Phys. Rev. Res.* **3**, 033275 (2021).
- [60] C. Oh, S.-Y. Lee, H. Nha, and H. Jeong, *Phys. Rev. A* **96**, 062304 (2017).
- [61] U. Chabaud, G. Roeland, M. Walschaers, F. Grosshans, V. Parigi, D. Markham, and N. Treps, *PRX Quantum* **2**, 020333 (2021).
- [62] B. Korzh *et al.*, *Nat. Photonics* **14**, 250 (2020).
- [63] W. H. P. Pernice, C. Schuck, O. Minaeva, M. Li, G. N. Goltsman, A. V. Sergienko, and H. X. Tang, *Nat. Commun* **3**, 1325 (2012).
- [64] T. Zhang, J. Huang, X. Zhang, C. Ding, H. Yu, Y. Xiao, C. Lv, X. Liu, Z. Wang, L. You, *et al.*, *Photonics Research* **12**, 1328 (2024).
- [65] M. Uria, P. Solano, and C. Hermann-Avigliano, *Phys. Rev. Lett.* **125**, 093603 (2020).
- [66] M. Cosacchi, J. Wiercinski, T. Seidelmann, M. Cygorek, A. Vagov, D. E. Reiter, and V. M. Axt, *Phys. Rev. Res.* **2**, 033489 (2020).
- [67] N. Jornod, M. Jankowski, L. M. Krüger, V. J. Wittwer, N. Modsching, C. Langrock, C. R. Phillips, U. Keller, T. Südmeyer, and M. M. Fejer, in *CLEO 2023* (Optica Publishing Group, 2023) p. STu3L.3.
- [68] K. Wakui, Y. Tsujimoto, M. Fujiwara, I. Morohashi, T. Kishimoto, F. China, M. Yabuno, S. Miki, H. Terai, M. Sasaki, and M. Takeoka, *Opt. Express* **28**, 22399 (2020).
- [69] Y. Liu, J. Zhao, Z. Wei, F. X. Kärtner, and G. Chang, *Opt. Lett.* **48**, 1052 (2023).
- [70] Y.-R. Chen, H.-Y. Hsieh, J. Ning, H.-C. Wu, H. L. Chen, Z.-H. Shi, P. Yang, O. Steuernagel, C.-M. Wu, and R.-K. Lee, “Generation of heralded optical ‘schroedinger cat’ states by photon-addition,” (2023), [arXiv:2306.13011 \[quant-ph\]](https://arxiv.org/abs/2306.13011).
- [71] R. Cheng, Y. Zhou, S. Wang, M. Shen, T. Taher, and H. X. Tang, *Nat. Photon.* **17**, 112 (2023).
- [72] N. C. Menicucci, P. van Loock, M. Gu, C. Weedbrook, T. C. Ralph, and M. A. Nielsen, *Phys. Rev. Lett.* **97**, 110501 (2006).
- [73] M. Endo, R. He, T. Sonoyama, K. Takahashi, T. Kashiwazaki, T. Umeki, S. Takasu, K. Hattori, D. Fukuda, K. Fukui, K. Takase, W. Asavanant, P. Marek, R. Filip, and A. Furusawa, *Opt. Express* **31**, 12865 (2023).
- [74] M. Endo, T. Nomura, T. Sonoyama, K. Takahashi, S. Takasu, D. Fukuda, T. Kashiwazaki, A. Inoue, T. Umeki, R. Nehra, P. Marek, R. Filip, K. Takase, W. Asavanant, and A. Furusawa, “High-rate four photon subtraction from squeezed vacuum: Preparing cat state for optical quantum computation,” (2025), [arXiv:2502.08952 \[quant-ph\]](https://arxiv.org/abs/2502.08952).